East Asian Journal on Applied Mathematics
doi: 10.4208/eajam.2023-045.090523

Vol. **xx**, No. x, pp. 1-37
xxx 2024

Advection-Pressure Splitting Schemes for the Equations of Blood Flow. Conservative and Non-Conservative Forms

Eleuterio F. Toro[1], Annunziato Siviglia[1,*], Alessandra Spilimbergo[2] and Lucas O. Müller[2]

[1]*Laboratory of Applied Mathematics, DICAM, University of Trento, Italy.*
[2]*Department of Mathematics, University of Trento, Italy.*

Received 1 February 2023; Accepted (in revised version) 9 May 2023.

Abstract. We present a class of simple advection-pressure splitting numerical methods to solve the blood flow equations in compliant arterial vessels. The schemes are inspired by the TV flux vector splitting approach for conservative systems, proposed by Toro and Vázquez [30]. But the reformulated TV-type splitting schemes of this paper have a wider range of applicability, including systems of equations in non-conservative form. The spatial differential operator is split into advection terms, which may be in conservative form, from pressure terms in conservative or non-conservative form. Additionally, unlike the original TV scheme, the reformulated splitting of this paper fully preserves the continuity equation as part of the pressure system. This last feature is consistent with zero-dimensional models for blood flow that are based on neglecting the inertial term in the momentum equation. The schemes are also well suited for systems in which geometric and biomechanical parameters of the problem vary discontinuously. The splitting schemes of this paper are systematically assessed on a carefully designed suite of test problems and compared with several existing, mainstream methods. Overall, the proposed numerical methods perform very satisfactorily and suggest themselves as attractive computational tools for modelling the dynamics of bodily fluids under realistic conditions.

AMS subject classifications: 65M08, 76Z05

Key words: Blood flow, hyperbolic equations, finite volume method, path-conservative method, TV splitting.

1. Introduction

This paper is concerned with a class of simple numerical methods for solving a system of hyperbolic partial differential equations (PDEs) that govern the fluid dynamics of

*Corresponding author. *Email addresses:* eleuterio.toro@unitn.it (E.F. Toro), annunziato.siviglia@unitn.it (A. Siviglia), a.spilimbergo@unitn.it (A. Spilimbergo), lucas.muller@unitn.it (L.O. Müller)

blood in compliant arterial vessels. The one-dimensional PDEs of interest depend on time t and distance x along the vessel and, despite its apparent simplicity, they account for the dynamics of blood inside the vessel, coupled to the simultaneous movement of the vessel wall. Blood vessel walls are not rigid, fixed boundaries. In other words, the alluded equations constitute a simplified fluid-structure interaction (FSI) model. Single vessel segments can be coupled to multiple segments through appropriate coupling conditions so as to form networks of blood vessels that may realistically emulate the circulatory system of mammals. Designing useful numerical methods to solve the equations may pose some challenges. To start with, the hyperbolic character of the equations admits solutions with large spatial and temporal gradients of the unknowns, including shocks, or more specifically, elastic jumps. Moreover, the PDEs include geometrical and biomechanical parameters, which in turn depend on distance along the vessel. Apart from the difficulty of determining such parameters, these may exhibit large spatial gradients, including discontinuities. Such geometrical and biomechanical parameters enter the equations in the form of algebraic source terms and add new features to the PDEs, such as stationary contact discontinuities. Such features constitute additional challenges to the algorithm designer, and the well-balanced concept enters the task of algorithm design. Extending the basic PDEs to account for these features and for some additional physics, such as viscoelasticity, causes the PDEs to loose their conservation-law form, forcing the algorithm designer to consider methods for non-conservative systems. Much progress has been made in the last few decades in the design of numerical method for evolutionary PDEs, notably hyperbolic equations. See for example the textbooks of Godlewski and Raviart [7], LeVeque [10] and Toro [22,23]. Such advances have permeated into various fields of application, including computational haemodynamics [4, 15]. In spite of significant progress in this field there are still plenty of challenges to overcome, including the formulation of approaches that embrace both conservative and non-conservative forms of the PDEs, and ability to extend the schemes to high-order of accuracy in both space and time. Simplicity of the algorithms is a highly desirable property, provided, of course, that accuracy and robustness are not sacrificed.

In this paper we present new computational algorithms to solve the cross-sectional averaged blood flow equations for blood flow in arterial vessels obeying an elastic closure condition, the tube law. Main features of the proposed schemes include (i) their ability to admit discontinuous geometric and biomechanical parameters, (ii) their ability to treat both the conservative and non-conservative forms of the equations and (iii) simplicity. The schemes presented in this paper build upon two existing approaches. The first concerns a flux vector splitting (FVS) method, along the lines of the classical FVS schemes due to Steger and Warming [19], van Leer [32], Liou and Steffen [11], Zha and Bilgen [33], and the more recent FVS of Toro and Vázquez [30]. An analogous, but different, splitting scheme was proposed in [21] to discretise the equations of compressible multiphase flow; in this approach the flux vector was split into several subsets of components, one for each phase, in order to compute a single numerical flux for all phases and then update all phases simultaneously. One may term this splitting approach phase splitting. As the term splitting appears in several contexts, a word of caution is in order. First, these flux vector splitting approaches are distinct from time-splitting methods to treat source terms, or dimensional

splitting to treat multidimensional problems, for which the second-order Strang splitting is well known [20]. Flux vector splitting methods split the flux vector, either term by term, or component by component in the case of multiphase flow, to compute the full numerical flux in a simple manner, which, once available, permits the simultaneous updating the PDEs unknowns in a single time step. We note that one could also re-interpret the FVS methods as done in time splitting and dimensional splitting. But the accuracy of such approach would be at most two, if a Strang-type scheme is deployed.

The flux vector splitting schemes of this paper build upon the FVS method of Toro and Vázquez, called the TV splitting [30], originally proposed for the conservative Euler equations of compressible gas dynamics. In the TV splitting, as in most FVS methods, the flux vector is split into advection terms and pressure terms. But the TV approach differs from previous FVS approaches in two respects. First, the pressure operator includes all pressure terms, and second, the advection and pressure operators are used to formulate two simpler systems of PDEs that allow the computation of the complete numerical flux in a simple manner. In order to design TV-type methods for the blood flow equations, the original TV splitting must be modified in various ways. The first regards the continuity equation. In the original TV splitting this equation is entirely assigned to the advection system. In the present paper the continuity equation is fully assigned to the pressure system. This choice may be justified by the fact that in the construction of zero-dimensional simplifications to the blood flow equations, in which the inertial term in the momentum equation is neglected, the continuity equation is fully preserved, as in the present reformulation of the TV splitting. Another new feature of the TV approach of this paper, respect to the original TV scheme in [30], regards the admitted forms of the equations, namely both conservative and non-conservative forms. The non-conservative form appears naturally when admitting blood vessels of variable geometric and mechanical properties, and when admitting viscoelastic tube laws. In this case there is no flux vector in the equations, though there are still advection and pressure terms, to which the splitting is applied. Hence, one may speak of Advection-Pressure Splitting, which applies to both the conservative and non-conservative cases. The underlying framework of this paper is the Godunov-type path-conservative scheme of Parés and Muñoz [14]. This approach, originally formulated for purely non-conservative systems, is extended here to allow for advection terms in conservative form and pressure terms in non-conservative form. Some of these ideas were successfully implemented for the shallow water equations in Toro *et al.* [27] and to sediment transport in Siviglia *et al.* [18].

Summing up, the numerical schemes developed in the present paper depart from the new advection-pressure splitting approach and are applied to the blood flow equations for flow in arterial vessels obeying an elastic tube law. The governing equations may be written either in conservative or non-conservative form and admit the possibility of discontinuous geometric and mechanical properties. Up to this point the schemes are of first-order of accuracy and monotone, monotone for the scalar case, strictly speaking. Extension of the schemes to high order of accuracy is not addressed in the present paper; this task may be accomplished through the deployment of standard semi-discrete or fully discrete approaches. The constructed numerical schemes of this paper are systematically assessed

on a carefully designed suite of test problems with exact solution. Moreover, the assessment of the new methods includes comparison with several competitive numerical methods to solve the same problems, which include the Godunov method with the exact Riemann solver [8], HLL [9], HLLC [25, 29], DOT (Dumbser-Osher-Toro) [2, 3, 12], Rusanov [16] and FORCE [26]. The rest of this paper is structured as follows. In Section 2 we review the blood flow equations and motivate the variant of the TV splitting approach adopted here. In Section 3 we present the new schemes for the conservative form of the equations, which include a detailed solution of the Riemann problem for the pressure system. In Section 4 we extend the schemes to the non-conservative case in the framework of path-conservative methods. In Section 5 we asses the performance of the proposed numerical methods via a suite of carefully designed test problems with exact solution and through comparison with several existing methods. Concluding remarks are found in Section 6.

2. Review of the Equations and Motivation

Here we first briefly review the classical one-dimensional equations for blood flow in arterial vessels. We then present two forms of expressing the equations, namely the conservative form and the non-conservative form. The section is ended with a motivation for the main theme of this paper, namely the flux splitting approach.

2.1. Basic one-dimensional equations

The fluid dynamics of blood inside a compliant blood vessel interacting with the displacement of the vessel wall, and allowing for the transport of a generic passive scalar, can be represented by the following non-linear, first-order system of partial differential equations (PDEs):

$$\begin{aligned} &\partial_t A + \partial_x(uA) = s_1 = 0, \\ &\partial_t(uA) + \partial_x(\alpha A u^2) + \frac{A}{\rho}\partial_x p = s_2 = -\frac{8\mu\pi q}{\rho A}, \\ &\partial_t(A\eta) + \partial_x(Au\eta) = s_3 = 0. \end{aligned} \tag{2.1}$$

The first two equations are respectively mathematical statements of the physical principles of conservation of mass and balance of momentum. The conserved quantities are cross-sectional area $A(x,t)$ and flow $q(x,t) = A(x,t)u(x,t)$, where $u(x,t)$ is the blood velocity. The third equation models the transport of a passive scalar $\eta(x,t)$ with the velocity $u(x,t)$ and may represent the concentration of a generic chemical species; the equation is expressed in conservation-law form with the aid of the continuity equation, producing a third conserved quantity $A\eta$. On the right hand side of (2.1), s_1, s_2 and s_3 represent source terms, generally given by algebraic (not differential) expressions. The source terms may change due to generalisations of the equations. The independent variables x and t represent distance and time. A rigorous derivation of the non-linear model (2.1) from the Navier-Stokes equations is carried out, for example, in [4]. In system (2.1) it is important to clearly distinguish between unknowns and parameters, as discussed below.

Unknowns and the tube law. The unknowns of system (2.1) are $A(x,t)$: cross-sectional area of the vessel at position x and time t; $u(x,t)$: the cross-sectional area averaged velocity of blood at a vessel cross section; $p(x,t)$: cross-sectional area averaged pressure of blood inside the vessel, and $\eta(x,t)$ is the concentration of a generic chemical species. System (2.1) has more unknowns than equations. Therefore, in order to close the system, an extra equation is required, called closure condition. In haemodynamics such closure condition is called tube law. In the model (2.1) the vessel wall is not rigid and the tube law (2.2) couples the elastic properties of the compliant vessel wall to the fluid dynamics inside the vessel, to account for an essential feature of blood flow, that is the displacement of the vessel wall. The choice of tube law depends on the mechanical properties of the vessel wall and therefore one must distinguish between arteries and veins, for example. In this paper we assume a simple, elastic tube law for arteries, namely

$$\begin{aligned} p(x,t) &= p_{ext}(x,t) + p_T(A;K), \\ p_T(A;K) &= K(x)\left(\sqrt{\frac{A}{A_0}} - 1\right), \\ K(x) &= \frac{\sqrt{\pi}}{(1-\nu^2)}\frac{E(x)h_0(x)}{\sqrt{A_0(x)}}. \end{aligned} \tag{2.2}$$

Here $p_{ext}(x,t)$ is the external pressure and $p_T(A;K)$ is the transmural pressure, the difference between internal and external pressures, that is

$$p_T(A;K) = p(x,t) - p_{ext}(x,t).$$

In the arguments of the transmural pressure $p_T(A;K)$, note the distinction between unknowns and parameters, A is an unknown of the equations, while K is a parameter.

Parameters of the equations. The parameters of Eqs. (2.1)-(2.2) are ρ: density of blood, assumed to be a known constant, usually set to $\rho = 1050\ kg/m^3$; μ is blood viscosity, derived under the assumption of Newtonian fluid and assumed here to be a known constant; α is the Coriolis coefficient, assumed constant here; α is linked to the choice of velocity profile for one-dimensional representation of variables [6]; $A_0(x)$ is the cross-sectional area of the vessel at equilibrium, that is when the transmural pressures vanishes and $u = 0$; $h_0(x)$ is the vessel wall thickness; $E(x)$ is Young's modulus of elasticity; ν is the Poisson ratio, taken as $\nu = 1/2$ for incompressible media; $p_{ext}(x,t)$ is external pressure, assumed a prescribed function here. Note that in general the geometric and mechanical parameters $A_0(x)$, $h_0(x)$ and $E(x)$ vary with distance along the length of the vessel and are thus functions of x; $p_{ext}(x,t)$ may vary with both space and time. The determination of parameters is a major issue in computational haemodynamics and hence a source of uncertainties. Just for a moment, think of the task of determining the single function $h_0(x)$, or reconstructed versions of it, from measured data, for all vessels of the human cardiovascular system. Here we assume that all parameters are prescribed and the task is to find the unknowns by solving the system (2.1) of partial differential equations.

2.2. Conservative form and eigenstructure of the equations

Eqs. (2.1) can be recast in terms of different sets of unknowns and different forms. Regarding the form of the equations there are essentially two choices, namely the conservation-law form or conservative form, and the non-conservative form, as we shall explain. In what follows we shall assume that the parameters K, E, A_0, h_0 are constant. This assumption, even if not necessary, facilitates expressing the equations for blood flow in arteries in conservation-law form as follows:

$$\partial_t \mathbf{Q} + \partial_x \mathbf{F}(\mathbf{Q}) = \mathbf{S}(\mathbf{Q}), \tag{2.3}$$

where $\mathbf{Q}$ is the vector of unknowns, the conserved variables, $\mathbf{F}(\mathbf{Q})$ is the vector of fluxes and $\mathbf{S}(\mathbf{Q})$ is the source term vector (see [24] for more details on the derivation), all given as follows:

$$\begin{aligned}
\mathbf{Q} &= \begin{bmatrix} q_1 \\ q_2 \\ q_3 \end{bmatrix} \equiv \begin{bmatrix} A \\ Au \\ A\eta \end{bmatrix}, \\
\mathbf{F}(\mathbf{Q}) &= \begin{bmatrix} f_1 \\ f_2 \\ f_3 \end{bmatrix} \equiv \begin{bmatrix} Au \\ \alpha A u^2 + \gamma A^{3/2} \\ A\eta u \end{bmatrix}, \\
\mathbf{S}(\mathbf{Q}) &= \begin{bmatrix} s_1 \\ s_2 \\ s_3 \end{bmatrix} \equiv \begin{bmatrix} 0 \\ \dfrac{-8\pi\mu q}{\rho A} \\ 0 \end{bmatrix}.
\end{aligned} \tag{2.4}$$

The constant coefficient γ in (2.4) is given as

$$\gamma = \frac{K}{3\rho\sqrt{A_0}} = \frac{4\sqrt{\pi}}{9}\frac{Eh_0}{\rho A_0}.$$

For the rest of the paper we assume the Coriolis coefficient to be chosen as $\alpha = 1$. Eqs. (2.3) can also be written in non-conservative form as

$$\partial_t \mathbf{Q} + \mathbf{A}(\mathbf{Q})\partial_x \mathbf{Q} = \mathbf{S}(\mathbf{Q}),$$

where

$$\mathbf{A}(\mathbf{Q}) = \frac{\partial \mathbf{F}}{\partial \mathbf{Q}} = \begin{bmatrix} 0 & 1 & 0 \\ -u^2 + c^2 & 2u & 0 \\ -u\eta & \eta & u \end{bmatrix} \tag{2.5}$$

is the Jacobian matrix.

It is easily shown that the governing equations (2.3)-(2.4) are hyperbolic. The eigenvalues of the system are the eigenvalues of the Jacobian matrix (2.5), that is

$$\lambda_1 = u - c, \quad \lambda_2 = u, \quad \lambda_3 = u + c$$

with the wave speed c given as

$$c = \sqrt{\frac{A}{\rho}\frac{\partial p}{\partial A}} = \sqrt{\frac{3}{2}\gamma\sqrt{A}}.$$

The eigenvalues are all real and distinct provided $A > 0$. The corresponding right eigenvectors are

$$\mathbf{R}_1 = \beta_1 \begin{bmatrix} 1 \\ u-c \\ \eta \end{bmatrix}, \quad \mathbf{R}_2 = \beta_2 \begin{bmatrix} 0 \\ 0 \\ 1 \end{bmatrix}, \quad \mathbf{R}_3 = \beta_3 \begin{bmatrix} 1 \\ u+c \\ \eta \end{bmatrix},$$

where β_1, β_2 and β_3 are scaling factors, often chosen to be unity.

2.3. Motivation for the splitting schemes

The flux vector splitting approach of this paper is inspired by the TV splitting of Toro and Vázquez [30] for the Euler equations of compressible gas dynamics written in conservation-law form. In the TV splitting the flux function is split into an advection part and a pressure part that includes all pressure terms present in the equations. Moreover, in order to determine a numerical flux, the proposed TV splitting is invoked for formulating two systems of differential equations, one associated with the advection part of the flux, the advection system, and another associated with the pressure part, the pressure system. In the original TV splitting there is still freedom for selecting the advection variables. It turns out that for the blood flow equations of interest here, the choice that is productive differs from that for the Euler equations. Interestingly, it is the so-called zero-dimensional models, so popular in blood flow modelling, that provide a hint for choosing the advection operator, as we explain in what follows.

Zero-dimensional (0D) models in cardiovascular physiology can be traced back to the pioneering work of Otto Frank [5]. Such models are also called compartmental models or lumped-parameter models, or simply lumped models. The concept of compartment refers to a particular district of the body, or even a single blood vessel or segment of a vessel. Within each compartment, haemodynamics variables are constant in space (spatial homogeneity) and vary only in time. Zero-dimensional models may be constructed directly from one-dimensional models, such as system (2.1), by defining spatial integral averages in the appropriate compartment. In this manner the one-dimensional time dependent representation becomes a system of ordinary differential equations (ODEs) in time, for quantities that are spatially averaged in the chosen compartment.

In what follows we discuss a subsystem of PDEs contained in Eqs. (2.1) and (2.3)-(2.4) that is relevant to motivate the advection-pressure splitting proposed in this paper. Such subsystem actually arises from the construction of zero-dimensional ($0D$) models for blood flow. For details see [4,6], for example.

Conventionally zero-dimensional models depart [4,6] from the following subsystem of PDEs contained in Eqs. (2.1) and (2.3)-(2.4), namely

$$\begin{aligned} &\partial_t A + \partial_x(uA) = s_1 = 0, \\ &\partial_t(uA) + \frac{A}{\rho}\partial_x p = s_2 = -\frac{8\mu\pi q}{\rho A}. \end{aligned} \tag{2.6}$$

These equations result from (2.3)-(2.4) by neglecting the term $\alpha A u^2$ in the momentum equation. Spatial integral averaging of (2.6), assuming further simplifications of the tube law, results in a system of ODEs. This is achieved by first assuming a generic vessel segment $[x_1, x_2]$ of length $\Delta s = x_2 - x_1$ and defining integral averages

$$\begin{aligned} \hat{Q}(t) &= \frac{1}{\Delta s}\int_{x_1}^{x_2} q(x,t)dx, \\ \hat{p}(t) &= \frac{1}{\Delta s}\int_{x_1}^{x_2} p(x,t)dx, \\ \hat{A}(t) &= \frac{1}{\Delta s}\int_{x_1}^{x_2} A(x,t)dx. \end{aligned} \tag{2.7}$$

Then, it is assumed that (i) variations in the elasticity coefficient $K(x)$ in the tube law (2.2) are small and can thus be replaced by an averaged, constant K; (ii) variations of cross-sectional area $A(x,t)$ around the equilibrium cross-sectional area $A_0(x)$ are small; (iii) $A_0(x)$ is constant and denoted by A_0. After performing integration in (2.6), with definitions (2.7) one obtains a system of ODEs in time for the averaged cross-sectional area $\hat{A}(t)$ and averaged cross-sectional flow $\hat{Q}(t)$, namely

$$\begin{aligned} &\Delta s\frac{d}{dt}\hat{A}(t) + Q(x_2,t) - Q(x_1,t) = 0, \\ &\rho\frac{\Delta s}{A_0}\frac{d}{dt}\hat{Q}(t) + \rho\Omega\frac{\Delta s}{A_0^2}\hat{Q}(t) + p(x_2,t) - p(x_1,t) = 0, \quad \Omega = \frac{8\mu\pi}{\rho A_0}. \end{aligned} \tag{2.8}$$

All the assumptions made in deriving (2.8) are actually standard in realistic applications [4]. It is worth mentioning some recent work in which the strong assumptions alluded to are considerably relaxed [6, 17].

The community concerned with $0D$ models have analysed the consequences of neglecting the term $\alpha A u^2$ in the momentum equation of (2.1), or (2.3)-(2.4). In the dimensional analysis of Ghitti *et al.* [6], comparison was made of the size of the inertial term with that of the pressure term, in the full momentum equation in (2.3)-(2.4). The inertial term will be significantly smaller than the pressure term if $Fr = u^2/c^2$ is small, where Fr is a Froude number. Ghitti *et al.* [6] tested this condition on data from two well-known arterial vessel networks and concluded that Fr is small for a useful range of flow conditions in blood flow dynamics. For flow conditions outside this range one must return to the full equations (2.3)-(2.4).

From the point of view of the present paper, the discussion above has two implications: (i) the subsystem (2.6) has physical validity for non-trivial flow conditions and naturally furnishes a vector that results in the sought pressure system in the framework of the TV

splitting of [30], (ii) the limitations of (2.6) can be remedied by restoring the neglected inertial term, which in turn gives a vector that naturally results in the sought advection system. In other words, the steps leading to the derivation of zero-dimensional models have lead us to the formulation of a TV-type flux vector splitting scheme for the blood flow equations. Moreover, out of many possible choices for the sought advection and pressure subsystems, the one emerging from this discussion is shown to be successful here. We note also that such approach has recently been shown to be successful for the shallow water equations [27] and for a model for sediment transport [18].

3. Flux Vector Splitting for the Conservative Form

For the conservative form (2.3)-(2.4) of the equations, we adopt the conservative numerical scheme

$$\mathbf{Q}_i^{n+1} = \mathbf{Q}_i^n - \frac{\Delta t}{\Delta x}\left(\mathbf{F}_{i+1/2} - \mathbf{F}_{i-1/2}\right) + \Delta t \mathbf{S}_i, \tag{3.1}$$

where the numerical flux $\mathbf{F}_{i+1/2}$ and the numerical source $\mathbf{S}_i$ must be specified in order to fully define scheme (3.1). The computation of the numerical flux $\mathbf{F}_{i+1/2}$ is motivated by the discussion in the previous section. We split the flux vector into an advection part and a pressure part, as detailed below.

3.1. Advection-pressure splitting

We depart from the 1D augmented equations for blood flow in arteries, written in conservation-law form (2.3)-(2.4). The TV splitting has two parts. First, we split the flux vector as

$$\mathbf{F}(\mathbf{Q}) = \mathscr{A}(\mathbf{Q}) + \mathscr{P}(\mathbf{Q}) \tag{3.2}$$

with

$$\mathbf{Q} = \begin{bmatrix} A \\ Au \\ A\eta \end{bmatrix}, \quad \mathscr{A}(\mathbf{Q}) = \begin{bmatrix} 0 \\ Au^2 \\ A\eta u \end{bmatrix}, \quad \mathscr{P}(\mathbf{Q}) = \begin{bmatrix} Au \\ \gamma A^{3/2} \\ 0 \end{bmatrix}. \tag{3.3}$$

Here we have assumed the Coriolis coefficient to be unity, $\alpha = 1$ in Eqs. (2.3)-(2.4). $\mathscr{A}(\mathbf{Q})$ is called the advection flux and $\mathscr{P}(\mathbf{Q})$ is called the pressure flux. Second, we make use of the two fluxes $\mathscr{A}(\mathbf{Q})$ and $\mathscr{P}(\mathbf{Q})$ to formulate two distinct systems of PDEs, namely

$$\begin{aligned} &\text{Advection system:} \quad \partial_t \mathbf{Q} + \partial_x \mathscr{A}(\mathbf{Q}) = \mathbf{0}, \\ &\text{Pressure system:} \quad \partial_t \mathbf{Q} + \partial_x \mathscr{P}(\mathbf{Q}) = \mathbf{0}. \end{aligned} \tag{3.4}$$

The aim of the second step is to exploit each sub-system so as to obtain corresponding numerical fluxes $\mathscr{A}_{i+1/2}$, the advection numerical flux, and $\mathscr{P}_{i+1/2}$, the pressure numerical flux. The complete numerical flux for the full system (2.3)-(2.4) will be given as

$$\mathbf{F}_{i+1/2} = \mathscr{A}_{i+1/2} + \mathscr{P}_{i+1/2}, \tag{3.5}$$

which will then used in the conservative scheme (3.1). We note that the source terms may, in principle, be assigned to any of the systems in (3.4).

Remarks:

1. We note that the above flux splitting (3.2)-(3.3) differs from the original TV splitting [30], as remarked earlier in Section 2.3. Here, we assign the continuity equation fully to pressure system in (3.4).

2. The present version is consistent with approximations to the full equations in which the inertial term is neglected, leading to an approximation that coincides with the pressure system in (3.4).

3. This splitting is also consistent with zero-dimensional approximation to the blood flow equations, in which one effectively replaces the pressure system of PDEs in (3.4) by a system of ordinary differential equations (2.8) in time, by integrating the system in space, in a control volume, see Section 2.3.

4. As a matter of fact the pressure PDE system in (3.4) could well be proposed as a PDE system to model flow under very subcritical conditions, that is for Fr small, instead of the simplified, integrated ODE system (2.8). In addition to blood, the model may also be useful for other physiological fluids, such as lymph.

The numerical strategy to determine the advection and pressure numerical fluxes in (3.5) relies on first solving the Riemann problem for the pressure system in (3.4). The solution of this system will fully determine the pressure numerical flux $\mathscr{P}_{i+1/2}$ and will also provide advection information for determining the advection numerical flux $\mathscr{A}_{i+1/2}$ in (3.5). In other words, we only need to solve the Riemann problem for the pressure system in (3.4). This is carried out in the next section.

3.2. The pressure system

As the pressure system arising from the TV-type splitting applied to the blood flow equations is new in the literature, we perform here a fairly detailed analysis, starting from some mathematical properties of the equations. The governing equations of the pressure system are

$$\partial_t \mathbf{Q} + \partial_x \mathscr{P}(\mathbf{Q}) = \mathbf{0} \tag{3.6}$$

with definitions

$$\mathbf{Q} = \begin{bmatrix} A \\ Au \\ A\eta \end{bmatrix}, \quad \mathscr{P}(\mathbf{Q}) = \begin{bmatrix} Au \\ \gamma A^{3/2} \\ 0 \end{bmatrix}. \tag{3.7}$$

Source terms have been ignored, as they are not relevant to the subject of this section. The eigenvalues of system (3.6)-(3.7) are all real and distinct and given as

$$\lambda_1 = -c, \quad \lambda_2 = 0, \quad \lambda_3 = c.$$

The corresponding linearly independent right eigenvectors are

$$\mathbf{R}_1 = \begin{bmatrix} 1 \\ -c \\ 0 \end{bmatrix}, \quad \mathbf{R}_2 = \begin{bmatrix} 0 \\ 0 \\ 1 \end{bmatrix}, \quad \mathbf{R}_3 = \begin{bmatrix} 1 \\ c \\ 0 \end{bmatrix}.$$

The scaling factors have been set to unity. The pressure system is therefore hyperbolic. Note the subsonic (or subcritical) character of system (3.6)-(3.7), that is

$$\lambda_1 = -c < \lambda_2 = 0 < \lambda_3 = c.$$

It is straightforward to show that the λ_2-field is linearly degenerate, while the λ_1-field and the λ_3-fields are genuinely non-linear, for all states A, for the tube law (2.2) in use here.

3.2.1. Exact solution of the Riemann problem

The Riemann problem at the interface $x = x_{i+1/2}$, is defined as follows:

$$\begin{aligned} &\text{PDEs:} \quad \partial_t \mathbf{Q} + \partial_x \mathscr{F}(\mathbf{Q}) = \mathbf{0}, \\ &\text{ICs:} \quad \mathbf{Q}(x,0) = \begin{cases} \mathbf{Q}_L \equiv \mathbf{Q}_i^n, & \text{if} \quad x < x_{i+1/2}, \\ \mathbf{Q}_R \equiv \mathbf{Q}_{i+1}^n, & \text{if} \quad x > x_{i+1/2}. \end{cases} \end{aligned} \tag{3.8}$$

Fig. 1 shows the structure of the solution, where the subsonic character of the system is put in evidence by the two wave families associated with the eigenvalues $\lambda_1 = -c$ and $\lambda_3 = c$, see Eq. (3.13) regarding the solution in the star region and related remarks. Note that the unknown star state $\mathbf{Q}_*$ in the star region coincides with the Godunov state needed for intercell flux evaluation [23].

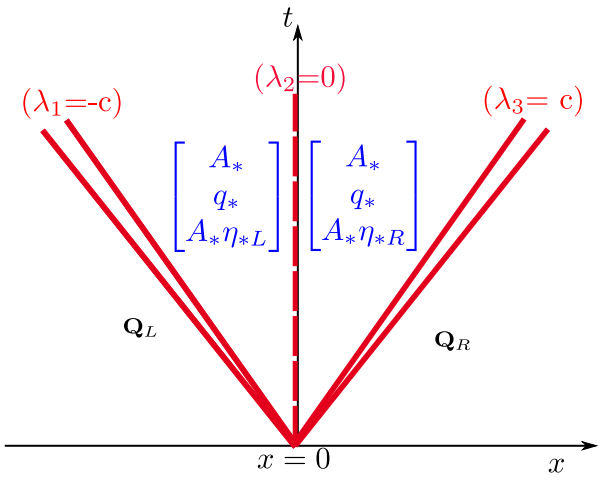

Figure 1: Structure of the solution of the Riemann problem (3.8) for the pressure system, in local coordinates, still called x and t, arising from the TV-type splitting. The structure of the wave system is symmetric, with a stationary contact discontinuity associated with the eigenvalue $\lambda_2 = 0$.

To solve the Riemann problem exactly we first proceed to study wave relations for each of the non-linear characteristic fields. See [23] for background on the methodology. We assume two types of non-linear waves, namely rarefaction waves and shock waves. We start from rarefaction waves.

Rarefaction waves. First, assume an isolated left-facing rarefaction wave associated with the eigenvalue $\lambda_1 = -c$, connecting the data state $\mathbf{Q}_L$ on the left to the unknown state $\mathbf{Q}_{*L}$ on the right. The generalised Riemann invariants [23] state that across the wave structure the following relations apply:

$$\frac{dA}{1} = \frac{dq}{-c} = \frac{d(A\eta)}{0}.$$

There follows

$$q + CA^{5/4} = \text{constant}, \quad A\eta = \text{constant} \tag{3.9}$$

with

$$C = \frac{4}{5}\sqrt{\frac{3}{2}\gamma}.$$

Analogously, the generalised Riemann invariants across a right-facing rarefaction are

$$\frac{dA}{1} = \frac{dq}{c} = \frac{d(A\eta)}{0},$$

which give

$$q - CA^{5/4} = \text{constant}, \quad A\eta = \text{constant}. \tag{3.10}$$

Application of (3.9) to connect $\mathbf{Q}_L$ on the left with $\mathbf{Q}_{*L}$ gives

$$q_* + CA_*^{5/4} = q_L + CA_L^{5/4}, \tag{3.11}$$

while application of (3.10) to connect $\mathbf{Q}_R$ on the right with $\mathbf{Q}_{*R}$ in the middle gives

$$q_* - CA_*^{5/4} = q_R - CA_R^{5/4}. \tag{3.12}$$

We note that exact integration leading (3.11) and (3.12) is possible for the tube law (2.2) used for arteries. For veins the situation is more complicated and integration must be performed numerically.

Remark: the contact discontinuity. Conventional eigenvector analysis of the λ_2-characteristic field reveals that all A, u and q are constant across the stationary contact discontinuity, unlike the passive scalar η that changes (discontinuously). That is

$$A_{*L} = A_{*R} = A_*, \quad u_{*L} = u_{*R} = u_*, \quad \eta_{*L} = \frac{A_L\eta_L}{A_*} \neq \eta_{*R} = \frac{A_R\eta_R}{A_*}. \tag{3.13}$$

Relations (3.13) justify the use of A_* in Eqs. (3.11)-(3.12).

In readiness for assembling the equations for the complete solution of the Riemann problem, from (3.11) we write

$$q_* = q_L - f_L(A_*; A_L), \quad f_L = C\left(A_*^{5/4} - A_L^{5/4}\right). \tag{3.14}$$

Analogously, from (3.12) we write

$$q_* = q_R + f_R(A_*; A_R), \quad f_R = C\left(A_*^{5/4} - A_R^{5/4}\right). \tag{3.15}$$

The two-rarefaction approximation. Under the a-priori assumption that both non-linear waves are rarefaction waves, direct application of (3.14)-(3.15) gives the exact solution in the star region

$$\begin{aligned} A_* &= \left[\frac{1}{2}\left(A_L^{5/4} + A_R^{5/4}\right) - \frac{1}{2C}(q_R - q_L)\right]^{4/5}, \\ q_* &= \frac{1}{2}(q_L + q_R) - \frac{1}{2}C\left(A_R^{5/4} - A_L^{5/4}\right), \\ \eta_{*L} &= \frac{A_L \eta_L}{A_*}, \quad \eta_{*R} = \frac{A_R \eta_R}{A_*}. \end{aligned} \tag{3.16}$$

If both non-linear waves happen to be rarefaction waves, then solution (3.16) is the exact solution. Otherwise it turns out to be a good approximation to the solution of the Riemann problem, also in the presence of shock waves (elastic jumps).

Shock waves. First we assume an isolated left-facing shock wave of speed S_L associated with the eigenvalue $\lambda_1 = -c$ connecting the data state $\mathbf{Q}_L$ on the left to $\mathbf{Q}_*$ on the right, behind the shock. Direct application of the Rankine-Hugoniot conditions gives

$$\begin{aligned} &S_L(A_* - A_L) = q_* - q_L, \\ &S_L(q_* - q_L) = \gamma\left(A_*^{3/2} - A_L^{3/2}\right), \\ &S_L(A_*\eta_* - A_L\eta_L) = 0. \end{aligned} \tag{3.17}$$

Manipulation of the first two equations gives

$$S_L = \pm\left[\frac{\gamma\left(A_*^{3/2} - A_L^{3/2}\right)}{(A_* - A_L)}\right]^{1/2}. \tag{3.18}$$

The correct choice of sign in (3.18) is yet to be made. From the first equation in (3.17) we may write

$$q_* = q_L + S_L(A_* - A_L).$$

Here we have chosen the negative sign on the grounds of the entropy condition

$$\lambda_1(\mathbf{Q}_L) > S_L > \lambda_1(\mathbf{Q}_*),$$

which implies

$$S_L < 0 \quad \text{and} \quad A_* > A_L.$$

In readiness for assembling the equations for the complete solution of the Riemann problem we write

$$q_* = q_L - f_L(A_*; A_L), \quad f_L = \Big[\gamma\big(A_* - A_L\big)\big(A_*^{3/2} - A_L^{3/2}\big)\Big]^{1/2}.$$

Analogous treatment of a right-facing shock wave of speed S_R associated to $\lambda_3 = c$ gives

$$q_* = q_R + f_R(A_*; A_R), \quad f_R = \Big[\gamma\big(A_* - A_R\big)\big(A_*^{3/2} - A_R^{3/2}\big)\Big]^{1/2}.$$

Collecting all results we obtain a single, non-linear algebraic equation for A_*, namely

$$f(A) = f_L + f_R + \Delta q = 0 \quad \text{with} \quad \Delta q = q_R - q_L, \tag{3.19}$$

where

$$f_L(A) = \begin{cases} C\left(A^{5/4} - A_L^{5/4}\right), & \text{if} \quad A \le A_L, \\ \Big[\gamma\big(A - A_L\big)\big(A^{3/2} - A_L^{3/2}\big)\Big]^{1/2}, & \text{if} \quad A > A_L, \end{cases}$$

$$f_R(A) = \begin{cases} C\left(A^{5/4} - A_R^{5/4}\right), & \text{if} \quad A \le A_R, \\ \Big[\gamma\big(A - A_R\big)\big(A^{3/2} - A_R^{3/2}\big)\Big]^{1/2}, & \text{if} \quad A > A_R. \end{cases}$$

Iterative solution for A_*. The nonlinear equation (3.19) is conveniently solved with an iterative Newton-Raphson method

$$A^{(k+1)} = A^{(k)} - \frac{f(A^{(k)})}{f'(A^{(k)})} \quad \text{for} \quad k = 0, 1, \ldots, k_{\max}. \tag{3.20}$$

The iterative process (3.20) is stopped whenever the change ΔA in A is smaller than a prescribed, small positive tolerance TOL, that is when

$$\Delta A \equiv \frac{|A^{(k+1)} - A^{(k)}|}{(A^{(k+1)} + A^{(k)})/2} < TOL. \tag{3.21}$$

Typically one chooses $TOL = 10^{-6}$ for single-precision calculations. As a guess value $A^{(0)}$ in (3.20) we use the two-rarefaction approximation (3.16). Inaccurate guess values for $A^{(0)}$ may cause the Newton-Raphson method to fail. Once the cross-sectional area $A = A_*$ has been found, the flow q_* is computed as

$$q_* = \frac{1}{2}(q_L + q_R) + \frac{1}{2}\big[f_R(A_*) - f_L(A_*)\big].$$

Then, the velocity in the Star Region follows as $u_* = q_*/A_*$. The solution for the passive scalar is $\eta_{*L} = A_L\eta_L/A_*$ and $\eta_{*R} = A_R\eta_R/A_*$. This follows from (3.16) for rarefaction waves and from (3.17) for shock waves. Note that across rarefaction waves $\eta(x,t)$ decreases smoothly; this follows from (3.9) and (3.10). Across a shock wave $\eta(x,t)$ decreases discontinuously.

3.3. Numerical fluxes

We have all the information required to compute the numerical fluxes in (3.5). First, for the pressure system we have two reliable choices for computing the pressure flux; the first choice is the non-iterative two-rarefaction solution (3.16). Numerous tests confirm that this approximation can be used with confidence in practice. Obviously, the second choice is the exact, iterative solution of (3.19), which has been presented in full detail here, as a reference solution. For the advection flux in (3.5) we simply use the advection information provided by the solution of the Riemann problem for the pressure system. Therefore, the TV-type split numerical fluxes are

$$\mathscr{P}_{i+1/2} = \begin{bmatrix} q_* \\ \gamma A_*^{3/2} \\ 0 \end{bmatrix}, \quad \mathscr{A}_{i+1/2} = \begin{cases} \begin{bmatrix} 0 \\ q_* u_L \\ q_* \eta_L \end{bmatrix}, & \text{if} \quad q_* \geq 0, \\ \begin{bmatrix} 0 \\ q_* u_R \\ q_* \eta_R \end{bmatrix}, & \text{if} \quad q_* < 0. \end{cases}$$

The sought full numerical flux is then given by (3.5), which can be used in the conservative formula (3.1) to update the complete system in one time step, in the full domain.

In the next section we deal with the case in which the equations are expressed in non-conservative form.

4. The Non-Conservative Case

For extensions of the equations for blood flow to tackle realistic applications, the governing equations cannot longer be written in conservation-law form, even if derived from physical conservation principles. This difficulty is also present in other fields of applications, notably in the simulation of compressible multiphase flows and sediment transport.

4.1. The framework

Here we tailor the TV-type splitting approach to solve systems of balance laws written in the form

$$\partial_t \mathbf{Q} + \partial_x \mathscr{A}(\mathbf{Q}) + \mathscr{M}(\mathbf{Q}) \partial_x \mathbf{Q} = \mathbf{S}(\mathbf{Q}). \tag{4.1}$$

This system has a conservative part $\partial_x \mathscr{A}(\mathbf{Q})$, a non-conservative part $\mathscr{M}(\mathbf{Q})\partial_x \mathbf{Q}$ and the source term $\mathbf{S}(\mathbf{Q})$. As written, the advection term is expressed in conservative form with flux function $\mathscr{A}(\mathbf{Q})$. Indeed, there is always the option of expressing the conservative advection term in non-conservative form via the chain rule, namely

$$\partial_x \mathscr{A}(\mathbf{Q}) = \frac{\partial \mathscr{A}}{\partial \mathbf{Q}} \partial_x \mathbf{Q} = \mathscr{B}(\mathbf{Q}) \partial_x \mathbf{Q}.$$

$\mathscr{B}(\mathbf{Q})$ is the Jacobian matrix of $\mathscr{A}(\mathbf{Q})$. Then, the full system (4.1) could be written in fully non-conservative form as

$$\partial_t \mathbf{Q} + \mathbf{A}(\mathbf{Q})\partial_x \mathbf{Q} = \mathbf{S}(\mathbf{Q}) \quad \text{with} \quad \mathbf{A}(\mathbf{Q}) = \mathscr{B}(\mathbf{Q}) + \mathscr{M}(\mathbf{Q}).$$

In this section we apply the TV-type splitting framework to the mixed form (4.1) and write two separate systems, as already done for the conservative case, namely

$$\begin{aligned} &\partial_t \mathbf{Q} + \partial_x \mathscr{A}(\mathbf{Q}) = \mathbf{0} \quad &: \text{ Conservative system for advection,} \\ &\partial_t \mathbf{Q} + \mathscr{M}(\mathbf{Q})\partial_x \mathbf{Q} = \mathbf{S}(\mathbf{Q}) \quad &: \text{ Non-conservative system for pressure.} \end{aligned} \tag{4.2}$$

In (4.2) we have allocated the source term $\mathbf{S}(\mathbf{Q})$ to the pressure system. However, there may be cases in which it is more convenient to allocate it to the advection system. In fact, this is an issue worth-investigating further.

4.2. Path-conservative approach

To tackle the non-conservative term in the mixed-formulation equations (4.1) we follow the path-conservative approach [1, 13, 31]. These schemes depend on the choice of a path ψ in phase space. In this framework we propose the mixed conservative/non-conservative simultaneous update numerical formula

$$\mathbf{Q}_i^{n+1} = \mathbf{Q}_i^n - \frac{\Delta t}{\Delta x}\left[\mathscr{A}_{i+1/2} - \mathscr{A}_{i-1/2}\right] - \frac{\Delta t}{\Delta x}\left[\mathbf{D}_{i-1/2}^{+} + \mathbf{D}_{i+1/2}^{-}\right] + \Delta t \mathbf{S}_i - \Delta t \mathbf{H}_i^n, \tag{4.3}$$

where

1. $\mathscr{A}_{i+1/2}$ is the numerical flux for the conservative part.
2. $\mathbf{D}_{i+1/2}^{\pm}$ are the fluctuations in the path-conservative scheme for the non-conservative part.
3. $\mathbf{S}_i$ is the numerical source.
4. $\mathbf{H}_i^n$ arises in schemes of accuracy greater than one and is defined as

$$\mathbf{H}_i^n = \frac{1}{\Delta t \Delta x}\int_{t_n}^{t_{n+1}} \int_{x_{i-1/2}}^{x_{i+1/2}} \mathbf{A}\big(\mathbf{P}_i(x,t)\big)\partial_x \mathbf{P}_i(x,t)\, dx dt.$$

   $\mathbf{P}_i(x,t)$ is a polynomial representation of the solution in cell I_i, which results from a spatial reconstruction procedure. In the first-order case of interest here, the reconstruction reduces to piece-wise constant cell averages. Hence, for first-order methods $\partial_x \mathbf{P}_i(x,t) = \mathbf{0}$ and therefore $\mathbf{H}_i^n = \mathbf{0}$ in (4.3). Nonetheless we keep $\mathbf{H}_i^n$ in the general path-conservative scheme (4.3) for the convenience of readers who might want to extend the method to high-order of accuracy.

The fluctuations $\mathbf{D}^-_{i+1/2}$ and $\mathbf{D}^+_{i+1/2}$, accounting for the absence of a flux function in the pressure system in (4.2), with coefficient matrix $\mathscr{M}(\mathbf{Q})$, are expected to satisfy the consistency condition

$$\mathbf{D}^-_{i+1/2}(\mathbf{Q},\dots,\mathbf{Q}) = \mathbf{0}, \quad \mathbf{D}^+_{i+1/2}(\mathbf{Q},\dots,\mathbf{Q}) = \mathbf{0}$$

and the compatibility condition

$$\mathbf{D}^-_{i+1/2} + \mathbf{D}^+_{i+1/2} = \int_0^1 \mathscr{M}\left(\mathbf{Q}\big(\psi(s;\mathbf{Q}^n_i,\mathbf{Q}^n_{i+1})\big)\right)\frac{\partial}{\partial s}\psi\big(s;\mathbf{Q}^n_i,\mathbf{Q}^n_{i+1}\big)ds.$$

The path function $\psi(s;\mathbf{Q}^n_i,\mathbf{Q}^n_{i+1})$, with $s\in[0,1]$, joins $\mathbf{Q}^n_i$ to $\mathbf{Q}^n_{i+1}$ and

$$\psi\big(0;\mathbf{Q}^n_i,\mathbf{Q}^n_{i+1}\big) = \mathbf{Q}^n_i, \quad \psi\big(1;\mathbf{Q}^n_i,\mathbf{Q}^n_{i+1}\big) = \mathbf{Q}^n_{i+1}.$$

While many choices for the path $\psi(s;\mathbf{Q}^n_i,\mathbf{Q}^n_{i+1})$ are available, here we assume the canonical path

$$\psi\big(s;\mathbf{Q}^n_i,\mathbf{Q}^n_{i+1}\big) = \mathbf{Q}^n_i + s\big(\mathbf{Q}^n_{i+1}-\mathbf{Q}^n_i\big). \tag{4.4}$$

In analogy to conservative methods, which require an intercell numerical flux $\mathbf{F}_{i+1/2}$ to be determined, path-conservative methods are defined once the path $\psi(s;\mathbf{Q}^n_i,\mathbf{Q}^n_{i+1})$ is specified and the fluctuations $\mathbf{D}^-_{i+1/2}$, $\mathbf{D}^+_{i+1/2}$ are determined.

The whole point of the TV splitting approach is its ability to provide simplified and effective schemes for computing the needed items in the numerical update formula (4.3), that is the fluctuations $\mathbf{D}^\pm_{i+1/2}$ and the numerical flux $\mathscr{A}_{i+1/2}$, as we shall see. There is also evidence, even if partial, that the TV splitting approach is advantageous in dealing with source terms, notably, of the discontinuous type. In this paper we implement the TV-type advection-pressure splitting in the framework of a convenient path-conservative scheme, which is presented next.

4.3. The Parés-Muñoz-Godunov scheme

Parés and Muñoz [14] proposed a Godunov-type, path-conservative method that results from the following definitions for the fluctuations:

$$\begin{aligned}
\mathbf{D}^-_{i+1/2} &= \int_0^1 \mathscr{M}\left(\psi\big(s;\mathbf{Q}^n_i,\mathbf{Q}_{i+1/2}(0)\big)\right)\frac{\partial}{\partial s}\psi\left(s,\mathbf{Q}^n_i,\mathbf{Q}_{i+1/2}(0)\right)ds,\\
\mathbf{D}^+_{i+1/2} &= \int_0^1 \mathscr{M}\left(\psi\big(s;\mathbf{Q}_{i+1/2}(0),\mathbf{Q}^n_{i+1}\big)\right)\frac{\partial}{\partial s}\,\psi\left(s,\mathbf{Q}_{i+1/2}(0),\mathbf{Q}^n_{i+1}\right)ds.
\end{aligned} \tag{4.5}$$

Here $\mathbf{Q}_{i+1/2}(x/t)$ denotes the solution of the Riemann problem

$$\begin{aligned}
&\partial_t\mathbf{Q} + \mathscr{M}(\mathbf{Q})\partial_x\mathbf{Q} = \mathbf{0},\\
&\mathbf{Q}(x,0) = \begin{cases}\mathbf{Q}^n_i, & \text{if} \quad x < x_{i+1/2},\\ \mathbf{Q}^n_{i+1}, & \text{if} \quad x > x_{i+1/2}\end{cases}
\end{aligned} \tag{4.6}$$

in local coordinates. $\mathbf{Q}_{i+1/2}(0)$ is the Godunov state, the determination of which requires solving the Riemann problem (4.6) to find $\mathbf{Q}_{i+1/2}(x/t)$ and a solution sampling procedure to determine $\mathbf{Q}_{i+1/2}(0)$.

A major undertaking here is to find a Riemann solver for (4.6), as for the non-conservative case there are less choices available than for the conservative case. The scheme just described will be denoted as the PMG scheme, for Parés, Muñoz and Godunov.

Implementing the PMG scheme. On the assumption that the Godunov state $\mathbf{Q}_{i+1/2}(0)$ is known, the implementation of the scheme proceeds as follows. Assuming the canonical paths (4.4) in (4.5) we have

$$\begin{aligned} \psi\left(s;\mathbf{Q}_i^n,\mathbf{Q}_{i+1/2}(0)\right) &= \mathbf{Q}_i^n + s\left[\mathbf{Q}_{i+1/2}(0)-\mathbf{Q}_i^n\right], \\ \psi\left(s;\mathbf{Q}_{i+1/2}(0),\mathbf{Q}_{i+1}^n\right) &= \mathbf{Q}_{i+1/2}(0) + s\left[\mathbf{Q}_{i+1}^n-\mathbf{Q}_{i+1/2}(0)\right]. \end{aligned} \tag{4.7}$$

Then, from (4.5) and (4.7) we have

$$\begin{aligned} \mathbf{D}_{i+1/2}^- &= \hat{\mathscr{M}}_{i+1/2}^-\left[\mathbf{Q}_{i+1/2}(0)-\mathbf{Q}_i^n\right], \\ \mathbf{D}_{i+1/2}^+ &= \hat{\mathscr{M}}_{i+1/2}^+\left[\mathbf{Q}_{i+1}^n-\mathbf{Q}_{i+1/2}(0)\right]. \end{aligned} \tag{4.8}$$

Here $\hat{\mathscr{M}}_{i+1/2}^-$ and $\hat{\mathscr{M}}_{i+1/2}^+$ are numerical approximations to respective integrals in (4.5), that is

$$\begin{aligned} \hat{\mathscr{M}}_{i+1/2}^- &\approx \int_0^1 \mathscr{M}\left(\psi\left(s;\mathbf{Q}_i^n,\mathbf{Q}_{i+1/2}(0)\right)\right) ds, \\ \hat{\mathscr{M}}_{i+1/2}^+ &\approx \int_0^1 \mathscr{M}\left(\psi\left(s;\mathbf{Q}_{i+1/2}(0),\mathbf{Q}_{i+1}^n\right)\right) ds. \end{aligned} \tag{4.9}$$

Using a Gaussian-Legendre rule to evaluate the integrals in (4.9) numerically we obtain

$$\begin{aligned} \hat{\mathscr{M}}_{i+1/2}^- &= \sum_{j=1}^{G} \omega_j \mathscr{M}\left(\psi\left(s_j;\mathbf{Q}_i^n,\mathbf{Q}_{i+1/2}(0)\right)\right), \\ \hat{\mathscr{M}}_{i+1/2}^+ &= \sum_{j=1}^{G} \omega_j \mathscr{M}\left(\psi\left(s_j;\mathbf{Q}_{i+1/2}(0),\mathbf{Q}_{i+1}^n\right)\right). \end{aligned} \tag{4.10}$$

For the integration points and weights, recommended choices are

$$s_1 = \frac{1}{2}-\frac{\sqrt{15}}{10}, \quad s_2 = \frac{1}{2}, \quad s_3 = \frac{1}{2}+\frac{\sqrt{15}}{10}, \quad \omega_1 = \frac{5}{18}, \quad \omega_2 = \frac{8}{18}, \quad \omega_3 = \frac{5}{18}.$$

The scheme, as formulated, is rather general. The specificity of the problem of interest will enter in resolving the pending task, namely finding a Riemann solver to determine the Godunov state $\mathbf{Q}_{i+1/2}(0)$ for use in (4.8) and (4.10).

Remark: there appears to be little reported experience on practical implementations of this kind of Godunov-type path-conservative methods. A recent application to the modelling of sediment transport in rivers is found in [18].

4.4. A non-conservative system from discontinuous parameters

A genuinely non-conservative system for blood flow results from a discontinuous stiffness coefficient K in (2.2). The system is written in the mixed form

$$\partial_t \mathbf{Q} + \partial_x \mathscr{A}(\mathbf{Q}) + \mathscr{M}(\mathbf{Q})\partial_x \mathbf{Q} = \mathbf{S}(\mathbf{Q}) \tag{4.11}$$

with

$$\begin{aligned} \mathbf{Q} &= \begin{bmatrix} A \\ Au \\ K \end{bmatrix}, \qquad \mathbf{S}(\mathbf{Q}) = \begin{bmatrix} 0 \\ s_2 - \dfrac{A}{\rho}\partial_x p_{ext} \\ 0 \end{bmatrix}, \\ \mathscr{A}(\mathbf{Q}) &= \begin{bmatrix} 0 \\ Au^2 \\ 0 \end{bmatrix}, \quad \mathscr{M}(\mathbf{Q}) = \begin{bmatrix} 0 & 1 & 0 \\ \dfrac{A}{\rho}\dfrac{\partial p}{\partial A} & 0 & \dfrac{A}{\rho}\dfrac{\partial p}{\partial K} \\ 0 & 0 & 0 \end{bmatrix}. \end{aligned} \tag{4.12}$$

Note that in this 3×3 model system there is no passive scalar equation. Instead, there is an equation for the parameter K following the approach proposed by Toro and Siviglia [28].

In order to solve system (4.11)-(4.12) numerically we shall use the scheme (4.3). This requires a numerical flux for advection part and fluctuations for the non-conservative pressure term. We do not address here, the task of devising general numerical schemes for the source terms, by exploiting the present splitting schemes. It turns out that the solution of the Riemann problem for the pressure system provides all the required items, namely the fluctuations and the numerical flux.

The pressure system from the TV splitting. The pressure system determines the fluctuations $\mathbf{D}^{\pm}_{i+1/2}$, but will also provide sufficient information to compute the numerical flux $\mathscr{A}_{i+1/2}$ for the advection term. We therefore study the pressure system in some detail. Consider the homogeneous version of the pressure system (4.11), namely

$$\partial_t \mathbf{Q} + \mathscr{M}(\mathbf{Q})\partial_x \mathbf{Q} = \mathbf{0}$$

with definitions (4.12). The eigenvalues of the matrix $\mathscr{M}(\mathbf{Q})$ are

$$\lambda_1 = -c, \quad \lambda_2 = 0, \quad \lambda_3 = c, \tag{4.13}$$

where c is the wave speed

$$c = \sqrt{\frac{A}{\rho}\frac{\partial p}{\partial A}}.$$

The corresponding right eigenvectors are

$$\mathbf{R}_1 = \begin{bmatrix} 1 \\ -c \\ 0 \end{bmatrix}, \quad \mathbf{R}_2 = \begin{bmatrix} D \\ 0 \\ -c^2 \end{bmatrix}, \quad \mathbf{R}_3 = \begin{bmatrix} 1 \\ c \\ 0 \end{bmatrix} \tag{4.14}$$

with

$$D = \frac{A}{\rho}\frac{\partial p}{\partial K}.$$

The scaling factors in the eigenvectors (4.14) have been assumed to be unity. Note the subsonic character of the pressure system, that is

$$\lambda_1 = -c < \lambda_2 = 0 < \lambda_3 = c.$$

The Riemann problem for the pressure system is

$$\begin{aligned} &\text{PDEs:} \quad \partial_t \mathbf{Q} + \mathscr{M}(\mathbf{Q})\partial_x \mathbf{Q} = \mathbf{0}, \quad -\infty < x < \infty, \quad t > 0, \\ &\text{ICs:} \quad \mathbf{Q}(x,0) = \begin{cases} \mathbf{Q}_L, & \text{if} \quad x < x_{i+1/2}, \\ \mathbf{Q}_R, & \text{if} \quad x > x_{i+1/2}. \end{cases} \end{aligned} \tag{4.15}$$

The initial data are the constant states $\mathbf{Q}_L$ and $\mathbf{Q}_R$. The structure of the solution is identical to that depicted in Fig. 1, though the solution is different, as we shall see. There are three wave families corresponding to the three eigenvalues (4.13). The sought Godunov state is precisely the star state, and hence no sampling is required to determine the sought information to compute the fluctuations. Note that the star state includes $\mathbf{Q}_{*L}$ and $\mathbf{Q}_{*R}$. The presentation of the exact Riemann solver for the pressure system (4.15) is omitted here. For background, the reader is referred to [23]. A detail to be noted. Although the equations are written in non-conservative form due to the jump in the coefficient of elasticity K, across the non-linear outer waves K is constant; therefore the Rankine-Hugoniot conditions are still applicable for the case of elastic jumps. See Section 3.2 for the conservative case and [23] for general background on solving Riemann problems.

Approximate Riemann solver. In what follows we seek an approximate solution based on the assumption that the two outer waves associated with $\lambda_1 = -c$ and $\lambda_3 = c$ are rarefaction waves. For algebraic convenience, in the tube law (2.2) we set

$$\sqrt{\frac{A}{A_0}} = \left(\frac{A}{A_0}\right)^m \quad \text{with} \quad m = \frac{1}{2}.$$

Across the λ_1 and λ_3 fields, the generalized Riemann invariants yield

$$\begin{aligned} q_* + T_L A_{*L}^{(m+2)/2} &= q_L + T_L A_L^{(m+2)/2}, \quad K_{*L} = K_L, \\ q_* - T_R A_{*R}^{(m+2)/2} &= q_R - T_R A_R^{(m+2)/2}, \quad K_{*R} = K_R \end{aligned}$$

with

$$T_L = \frac{2}{m+2}\sqrt{\frac{mK_L}{\rho A_0^m}}, \quad T_R = \frac{2}{m+2}\sqrt{\frac{mK_R}{\rho A_0^m}}.$$

Across the λ_2-field we have

$$dq = 0, \quad DdK + c^2 dA = 0 \;\; \rightarrow \;\; dp(A;K) = 0.$$

Therefore, the flow q and the pressure $p(A;K)$ are constant in the star region, that is

$$q_* : \text{constant}, \quad p_*(A;K) : \text{constant}.$$

Algebraic manipulations yield

$$\begin{aligned} &q_{*L} = q_{*R} = q_* : \text{constant}, \\ &A_{*L} = A_0 \left\{ \frac{K_R}{K_L}\left[\left(\frac{A_{*R}}{A_0} \right)^m - 1 \right] + 1 \right\}^{1/m}. \end{aligned}$$

There are three unknowns to be determined, namely q_*, A_{*L} and A_{*R}, which satisfy the following three equations:

$$\begin{aligned} &q_* + T_L A_{*L}^{(m+2)/2} = q_L + T_L A_L^{(m+2)/2}, \\ &q_* - T_R A_{*R}^{(m+2)/2} = q_R - T_R A_R^{(m+2)/2}, \\ &A_{*L} = A_0 \left\{ \frac{K_R}{K_L}\left[\left(\frac{A_{*R}}{A_0} \right)^m - 1 \right] + 1 \right\}^{1/m}. \end{aligned} \tag{4.16}$$

From the first and second equations in (4.16) we obtain

$$A_{*L} = \left[-\frac{T_R}{T_L} A_{*R}^{(m+2)/2} + \frac{1}{T_L}\left(q_L - q_R + T_L A_L^{(m+2)/2} + T_R A_R^{(m+2)/2} \right) \right]^{2/(m+2)}. \tag{4.17}$$

Combining (4.17) with the third equation in (4.16) we obtain a single algebraic equation for A_{*R}, namely

$$\begin{aligned} &f(A_{*R}) = A_0 \left\{ \frac{K_R}{K_L}\left[\left(\frac{A_{*R}}{A_0} \right)^m - 1 \right] + 1 \right\}^{1/m} - \left[-\frac{T_R}{T_L} A_{*R}^{(m+2)/2} + Z \right]^{2/(m+2)} = 0, \\ &Z = \frac{1}{T_L}\left(q_L - q_R + T_L A_L^{(m+2)/2} + T_R A_R^{(m+2)/2} \right). \end{aligned} \tag{4.18}$$

The non-linear algebraic equation (4.18) may be solved iteratively via a Newton-Raphson method, see (3.20)- (3.21). Having found A_{*R} we compute A_{*L} from (4.17), while q_* follows from (4.16) as

$$q_* = \frac{1}{2}\left(q_L + q_R + T_R A_{*R}^{(m+2)/2} - T_L A_{*L}^{(m+2)/2} + T_L A_L^{(m+2)/2} - T_R A_R^{(m+2)/2} \right).$$

The full solution in the star region is known, resulting in two star vectors, namely

$$\mathbf{Q}_{*L} = [A_{*L}, q_*, K_L]^T, \quad \mathbf{Q}_{*R} = [A_{*R}, q_*, K_R]^T.$$

4.5. Fluctuations and advection numerical flux

To compute the fluctuations we adopt the Parés-Muñoz-Godunov scheme (PMG) of Section 4.3. By defining the two Godunov states

$$\mathbf{Q}^{-}_{i+1/2}(0) = \mathbf{Q}_{*L}, \quad \mathbf{Q}^{+}_{i+1/2}(0) = \mathbf{Q}_{*R}$$

the PMG scheme computes the fluctuations as

$$\mathbf{D}^{-}_{i+1/2} = \hat{\mathscr{M}}^{-}_{i+1/2}\Big[\mathbf{Q}^{-}_{i+1/2}(0) - \mathbf{Q}^{n}_{i}\Big],$$
$$\mathbf{D}^{+}_{i+1/2} = \hat{\mathscr{M}}^{+}_{i+1/2}\Big[\mathbf{Q}^{n}_{i+1} - \mathbf{Q}^{+}_{i+1/2}(0)\Big]$$

with

$$\hat{\mathscr{M}}^{-}_{i+1/2} = \sum_{j=1}^{G} \omega_j \mathscr{M}\left(\psi\big(s_j; \mathbf{Q}^{n}_{i}, \mathbf{Q}^{-}_{i+1/2}(0)\big)\right),$$
$$\hat{\mathscr{M}}^{+}_{i+1/2} = \sum_{j=1}^{G} \omega_j \mathscr{M}\left(\psi\big(s_j; \mathbf{Q}^{+}_{i+1/2}(0), \mathbf{Q}^{n}_{i+1}\big)\right).$$

In computing the advection flux we shall directly utilise the available value q_* from the pressure system, so that

$$\mathscr{A}_{i+1/2} = \begin{bmatrix} 0 \\ q_* u_K \\ 0 \end{bmatrix}, \quad u_K = \begin{cases} u_L, & \text{if} \quad q_* \geq 0, \\ u_R, & \text{if} \quad q_* < 0. \end{cases}$$

Therefore, all the required items for the TV scheme (4.3) to solve system (4.11) are determined, namely the numerical flux $\mathscr{A}_{i+1/2}$ for the advection part in conservative form, and the fluctuations $\mathbf{D}^{-}_{i+1/2}$ and $\mathbf{D}^{+}_{i+1/2}$ for the non-conservative part.

Two classes of TV schemes are available. The first one, denoted as TV+PMG+Ex.RS, uses the TV splitting in the PMG path-conservative framework, along with the exact Riemann solver for the pressure system to find the Godunov state, fluctuations and the advection numerical flux. The second TV scheme is denoted as TV+PMG+Ap.RS, in which the exact Riemann solver is replaced by the approximate Riemann solver just described.

5. Test Problems and Numerical Results

In this section we design test problems and assess the performance of the TV-type splitting numerical methods presented in this paper, both for the conservative and non-conservative cases. Numerical results are compared with the exact solution and with the results from other competitive numerical methods in the literature.

5.1. The Conservative case

Here we specify test problems for the conservative form of the governing equations and assess the performance of the proposed TV-type splitting schemes.

5.1.1. Test problems

For the conservative case we select three test problems. The tests have been chosen so as to represent the main features of the admissible solutions of the blood flow equations, namely smooth solutions, large spatial gradients and discontinuous solutions in the form of elastic jumps and contact discontinuities. Initial data for all three test problems are given in Table 1, while parameter values for such tests are given in Table 2, for arteries. The initial conditions are given in terms of the physical variables A, u and η. Columns 2-4 give the initial data to the left of x_0, while columns 2-7 give respective values on the right hand side of x_0. The output time T_{out} at which results are displayed is given in column 7.

Numerical results will be shown for all the methods displayed in Table 3, including upwind and a centred method. The TV-type methods of this paper are assessed for two versions, namely that in conjunction with the exact Riemann solver (TV+Ex.RS) and that with an approximate Riemann solver (TV+Ap.RS). These are schemes 1 and 2 in Table 3.

Table 1: Initial data for three test problems for the augmented blood flow equations in conservation-law form. The 9-th column describes the wave pattern that emerges from the exact solution, where R stands for rarefaction, C stands for contact discontinuity and S stands for shock.

Test	A_L	u_L	η_L	A_R	u_R	η_R	T_{out}	Wave pattern
1	3.50e-04	0.00	1.00	3.00e-04	0.00	0.00	0.05	RCS
2	10.00e-04	0.00	1.00	1.00e-04	0.00	0.00	0.04	R(sonic)CS
3	3.14e-04	-0.50	1.00	3.14e-04	0.50	0.00	0.05	RCR

Table 2: Parameters for tests 1 to 3 in Table 1 for arteries. Here x_0 denotes position of the initial discontinuity, h_0 is vessel wall thickness, A_0 is equilibrium cross-sectional area, E is Young's modulus, ν is Poisson ratio and ρ is blood density. The units of measure are respectively s, m, Kg and Pa.

Domain length	x_0	α	h_0	A_0	E	ν	ρ
0.50	0.25	1.00	5.00e-04	3.14e-04	3.00e-05	0.50	1000

Table 3: Numerical schemes to be assessed by comparing their approximate solutions to the exact solution. The Acronym of column 2 will be used to identify the scheme in the figures displaying numerical results.

Scheme	Acronym	Description	Note
1	TV+Ex.RS	TV Split. with Ex. Riem. Solv. for Press. Syst.	Upwind
2	TV+Ap.RS	TV Split. with App. Riem. Solv. for Press. Syst.	Upwind
3	God+Ex.RS	Godunov method with exact Riem. Solv.	Upwind
4	DOT	Godunov with Dumbser-Osher-Toro Riem. Solv.	Upwind
5	HLLC	Godunov method with HLLC Riem. Solv.	Upwind
6	HLL	Godunov method with HLL Riem. Solv.	Upwind
7	Rusanov	Rusanov method	Upwind
8	FORCE	FORCE method	Centred

For comparison, six additional competitive methods are also included in the assessment of the new schemes. The Godunov method [8] used in conjunction with the exact Riemann solver is fully described in [23]. The DOT (Dumbser-Osher-Toro) method is described in [2, 3]. The schemes HLL [9], HLLC [25, 29], Rusanov [16] and FORCE [26] are all fully described in [23].

5.1.2. Numerical results

Computed results compared with the exact solution are shown in Figs. 2-7. Each figure displays results from four schemes, for a single test problem, for the cross-sectional area A, velocity u and passive scalar η.

Results from Test 1. Results are shown in Figs. 2 and 3. In Fig. 2 the two top frames show results from the TV-type splitting scheme of this paper in conjunction with the exact Riemann solver (TV+Ex.RS) and with the two-rarefaction approximate Riemann solver (TV+Ap.RS). The two bottom frames show results from the Godunov method in conjunction with the exact Riemann solver and from the DOT scheme. All approximations are accurate and very similar amongst themselves for the rarefaction wave, the contact and the shock wave. Fig. 3 shows numerical results from four methods (symbol) compared to the exact solution (line), namely HLLC, HLL, Rusanov and FORCE. All four numerical schemes give comparable results for the rarefaction wave and the shock wave, but differ significantly for the contact discontinuity. HLLC gives the best result, while the remaining schemes exhibit excessive numerical dissipation for the contact discontinuity. Recall that HLLC, HLL, and Rusanov are upwind schemes, while FORCE is a centred scheme. The TV-type schemes of Fig. 2 compare very well with the HLLC results of Fig. 3.

Results from Test 2. Results are shown in Figs. 4 and 5. In Fig. 4 the two top frames show results from the TV-type splitting scheme of this paper, in conjunction with the exact Riemann solver (TV+Ex.RS) and with the two-rarefaction approximate Riemann solver (TV+Ap.RS). The two bottom frames show results from the Godunov method in conjunction with the exact Riemann solver and from the DOT scheme. All approximations are accurate and very similar amongst themselves for the rarefaction wave, the contact and the shock wave. Note that the strong left rarefaction is transcritical, which is evident from the well-known entropy glitch computed by the Godunov method with the exact Riemann solver [23]. The DOT scheme exhibits an analogous behaviour at the critical point. The TV schemes do not show an entropy glitch at the critical point but exhibit more numerical diffusion than the other two schemes for the rarefaction wave. The resolution of the shock and the contact discontinuity is similar in all four schemes. Fig. 5 shows numerical results from four methods (symbol) compared to the exact solution (line), namely HLLC, HLL, Rusanov and FORCE. Surprisingly, the results from HLLC and HLL are very similar. One would have expected a difference in the resolution of the contact discontinuity. As expected, the results from Rusanov and FORCE are very similar and exhibit more numerical diffusion than HLLC and HLL. The results from the TV-type schemes of Fig. 4 compare very well with those from HLLC in Fig. 5.

Results from Test 3. Results are shown in Figs. 6 and 7. In Fig. 6 the two top frames show results from the TV-type splitting scheme of this paper in conjunction with the exact Riemann solver (TV+Ex.RS) and with the two-rarefaction approximate Riemann solver (TV+Ap.RS). The two bottom frames show results from the Godunov method in conjunction with the exact Riemann solver and from the DOT scheme. The main challenge for this test problem is the sharp resolution of the stationary contact discontinuity. Results from all schemes are comparable. The DOT schemes shows slight over and undershoots at the contact discontinuity. Fig. 7 shows numerical results from four methods (symbol) compared to the exact solution (line), namely HLLC, HLL, Rusanov and FORCE. All four numerical schemes give comparable results for the rarefaction waves. But for the contact discontinuity HLLC is the only scheme that gives a perfect resolution, while the remaining schemes exhibit excessive numerical dissipation. The results from the TV-type schemes of Fig. 6 compare very well with those of HLLC in Fig. 7.

5.2. The Non-Conservative case

In this section we assess the performance of the TV-type splitting schemes of this paper through two test problems for which the equations are written in non-conservative form. We compare results with the exact solution and with three other competitive path-conservative methods. Table 4 shows all four methods assessed. Details for the 4th method (DOT non-conservative well balanced) are found in [12].

Table 4: Path-conservative schemes for solving non-conservative systems.

Scheme	Name	Description	Note
1	TV+PMG+Ex.RS	TV Split. +PMG+Ex. RS. for Press. Syst.	Upwind
2	PMG+Ex.RS	Páres-Muñoz-Godunov and Ex. Riem. Solv.	Upwind
3	DOT+NC	Dumbser-Osher-Toro (DOT) non-conservative	Upwind
4	DOT+NC+WB	DOT non-conservative and well-balanced	Upwind

5.2.1. Test problems and parameters

We have selected two test problems with exact solution. Table 5 gives the initial conditions for A, u and K. The 8th column shows the output time, while the last column describes the wave pattern in the exact solution. Table 6 gives the values of parameters for each

Table 5: Initial data for non-conservative test problems 1 and 2, for the augmented equations for blood flow with discontinuous parameters. Data for A_L and A_R depend on $\hat{p}$ and data for K_L and K_R, respectively. Here $\hat{p} = 7999.32\,Pa$ and K_{ref} is given in Table 6.

Test	A_L	u_L	K_L	A_R	u_R	K_R	T_{out}	Wave Patt.
1	$A_L(\hat{p}; K_L)$	0.0	K_{ref}	$A_R(\hat{p}; K_R)$	0.0	$10K_{ref}$	0.005	Stationary
2	$0.7A_0$	1.0	K_{ref}	A_0	0.0	$10K_{ref}$	0.007	SCS

Table 6: Parameters for tests for non-conservative problems in Table 5. SI units of measure are used: s, m, Kg and Pa.

Parameter	Units	Test 1	Test 2
$A_{0,\text{ref}}$	m^2	3.1353e-04	3.1353e-04
K_{ref}	Pa	58725	58725
A_0	m^2	$A_{0,\text{ref}}$	$A_{0,\text{ref}}$
p_e	Pa	0.00	0.00
m	$-$	0.50	0.50
n	$-$	0.00	0.00
l	m	0.20	0.20
x_0	m	0.10	0.06
ρ	$\frac{kg}{m^3}$	1000	1000

test problem. The test problems chosen here are very demanding. First, the flow variables have discontinuous initial conditions (Riemann problems). In addition, the parameter K is variable; moreover, it changes discontinuously across the position x_0. The single parameter K accounts for the variation of other parameters, see Eq. (2.2). Even very sophisticated non-conservative methods are known to fail for this kind of problems.

5.2.2. Numerical results

Fig. 8 shows results for Test 1 (non-conservative) from four path-conservative methods (symbol) shown in Table 4, compared to the exact solution (line). The top two frames show results from the PMG approach. The left frame shows results from the TV-type splitting of this paper with the PMG approach in conjunction with the exact Riemann solver for the pressure system (TV+PMG+Ex.RS). The right frame shows results from PMG for the full system (no splitting) in conjunction with the exact Riemann solver for the full system (PMG+Ex.RS). The two bottom frames show results from the non-conservative version of the DOT scheme in non-well balanced form (DOT+NC) and with the non-conservative well-balanced version (DT+NC+WB). The results from our new TV-type splitting scheme are very satisfactory. The discontinuous stationary middle wave (contact discontinuity) is captured perfectly, as a true discontinuity and without spurious oscillations. Two of the other path-conservative methods also perform very satisfactorily. Note however that even the sophisticated DOT path-conservative method fails, unless the well-balanced property is incorporated into the scheme, in which case the results match those of the new scheme. To our knowledge, the scheme PMG+Ex.RS (Páres-Muñoz-Godunov and exact Riemann solver) is new and represents the analogue of the Godunov scheme with exact Riemann solver for the conservative case. The contact discontinuity is preserved as a true discontinuity with no spurious oscillations.

Fig. 9 shows results for Test 2 (non-conservative) from four path-conservative methods (symbol) shown in Table 4, compared with the exact solution (line). The top two frames show results from the PMG approach. The left frame shows results from the TV-type split-

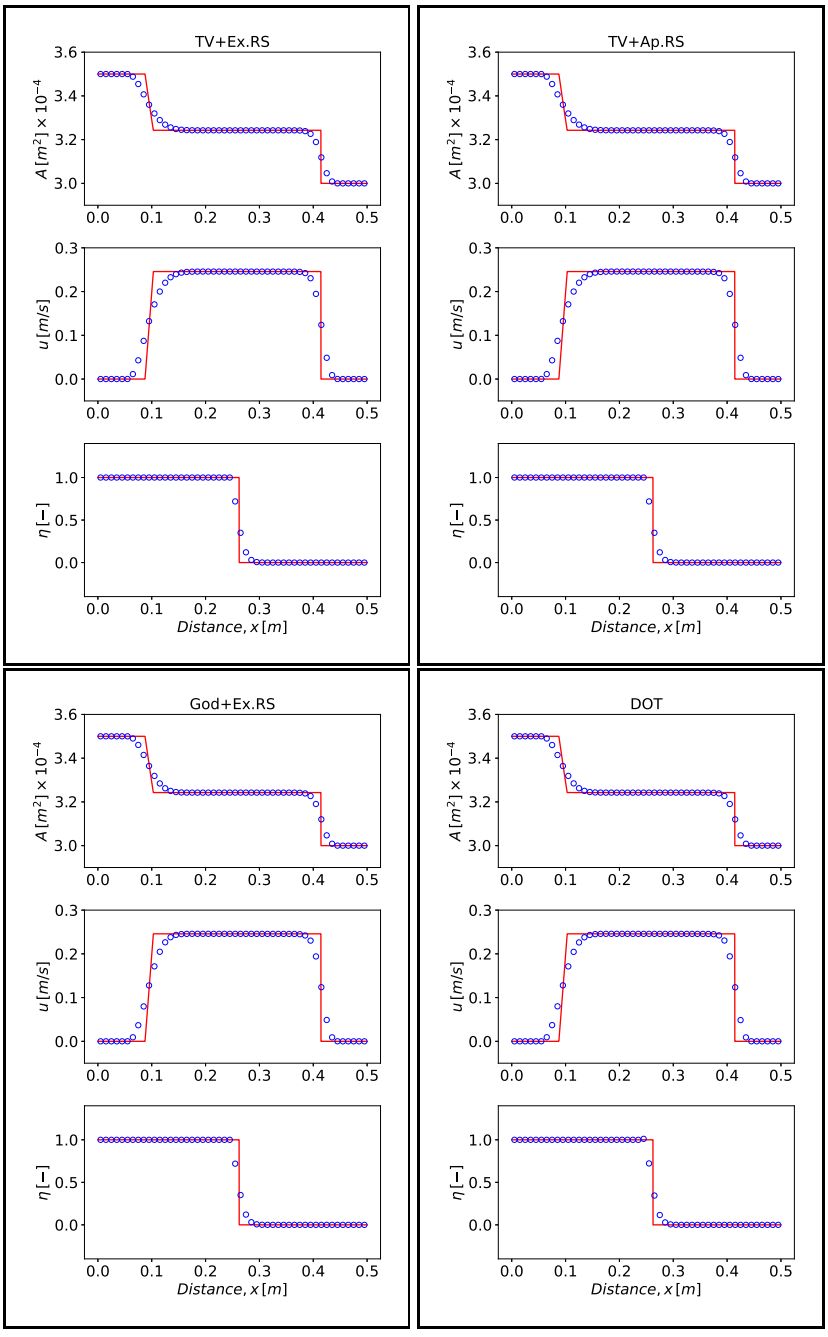

Figure 2: Test 1. Conservative case. Numerical solution from four conservative methods (symbol) compared to the exact solution (line). The top two frames show results from the TV-type splitting scheme of this paper in conjunction with the exact Riemann solver (TV+Ex.RS) and an approximate Riemann solver (TV+Ap.RS). The two bottom frames show results from the Godunov method used in conjunction with the exact Riemann solver and from the DOT scheme. $M = 50$ cells, $C_{cfl} = 0.9$. Initial data is given in Table 1 and parameters are given in Table 2.

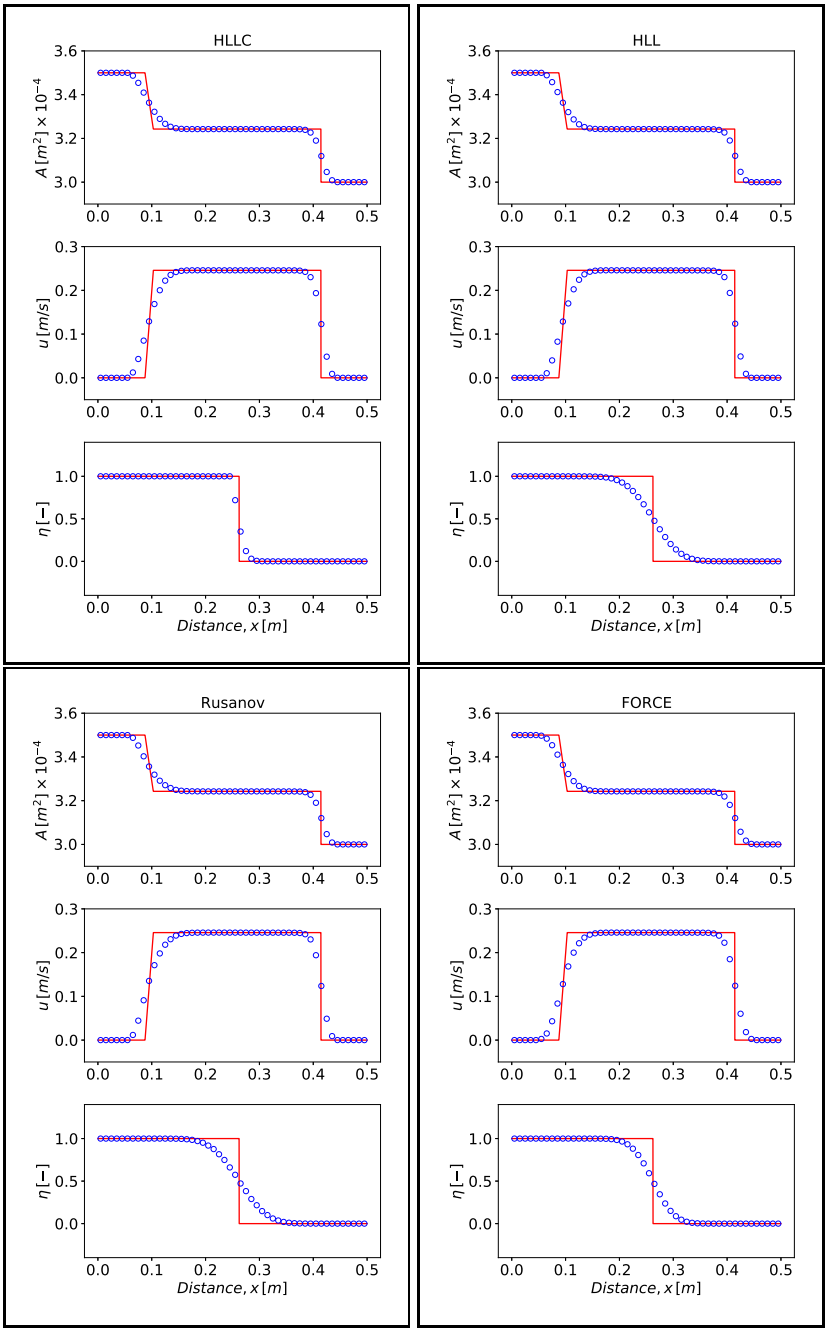

Figure 3: Test 1. Conservative case. Numerical solution from four conservative methods (symbol) compared to the exact solution (line). The top two frames show results from the HLLC and HLL schemes. The two bottom frames show results from the Rusanov and the FORCE scheme. $M = 50$ cells, $C_{cfl} = 0.9$. Initial data is given in Table 1 and parameters are given in Table 2.

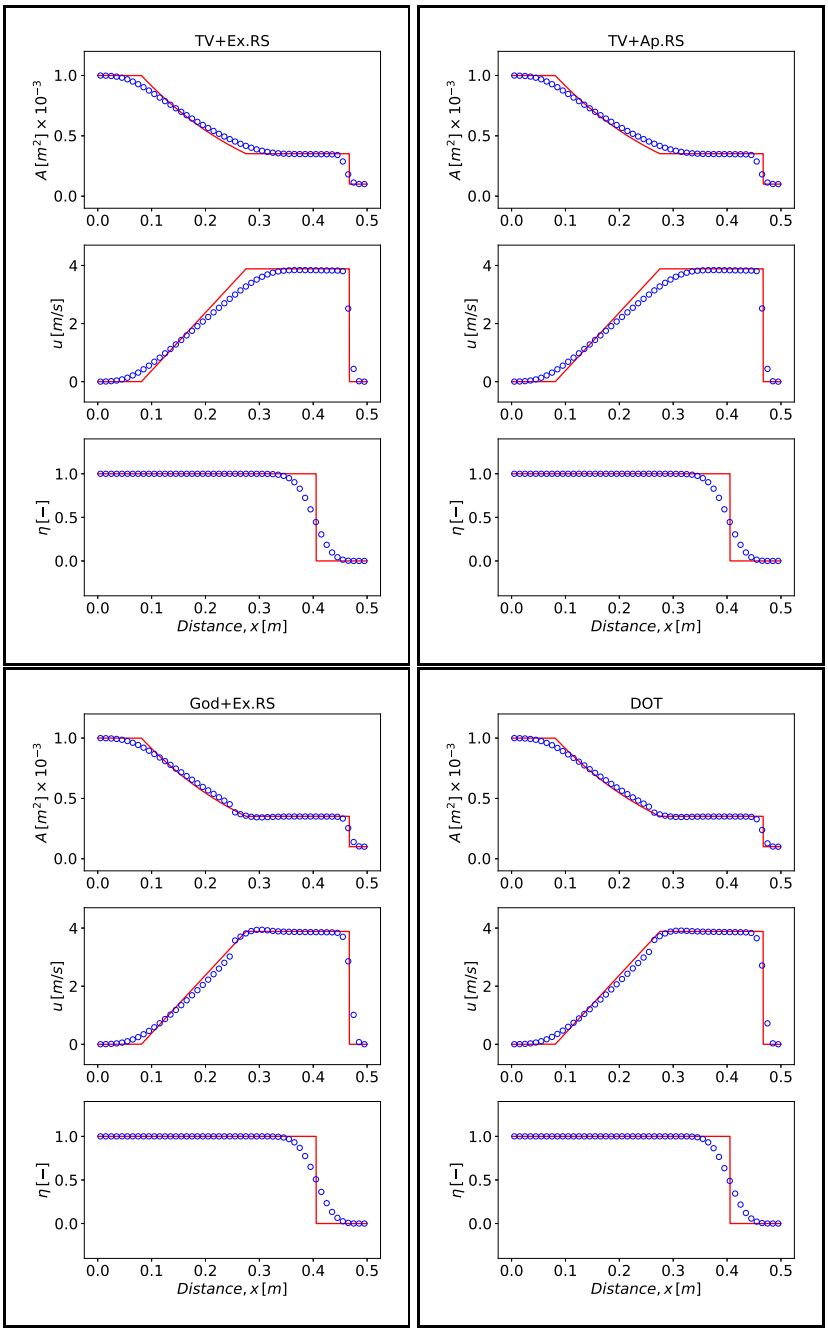

Figure 4: Test 2. Conservative case. Numerical solution from four conservative methods (symbol) compared to the exact solution (line). The top two frames show results from the TV-type splitting scheme of this paper in conjunction with the exact Riemann solver (TV+Ex.RS) and an approximate Riemann solver (TV+Ap.RS). The two bottom frames show results from the Godunov method used in conjunction with the exact Riemann solver and from the DOT scheme. $M = 50$ cells, $C_{cfl} = 0.9$. Initial data is given in Table 1 and parameters are given in Table 2.

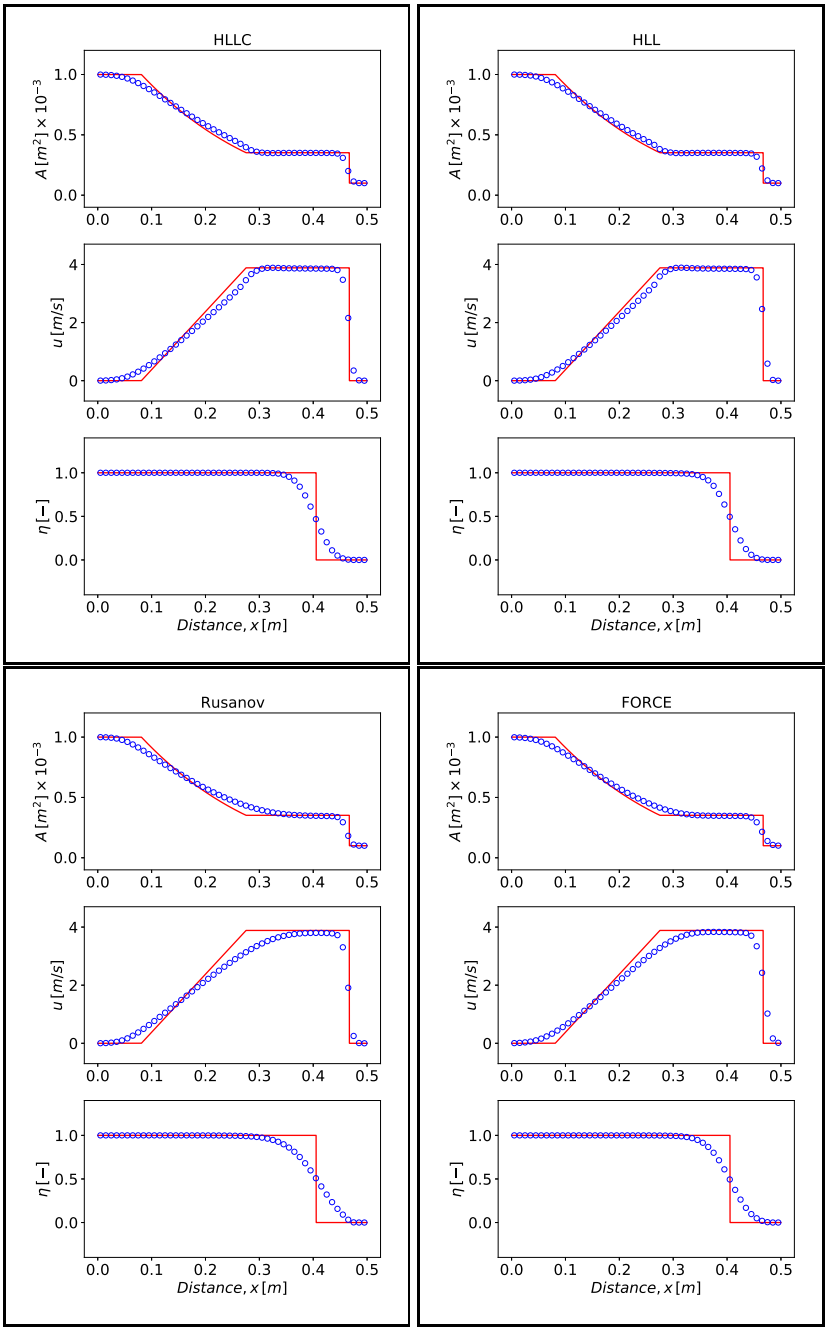

Figure 5: Test 2. Conservative case. Numerical solution from four conservative methods (symbol) compared to the exact solution (line). Top frames show results from the HLLC and HLL schemes. The two bottom frames show results from the Rusanov and the FORCE scheme. $M = 50$ cells, $C_{cfl} = 0.9$. Initial data is given in Table 1 and parameters are given in Table 2.

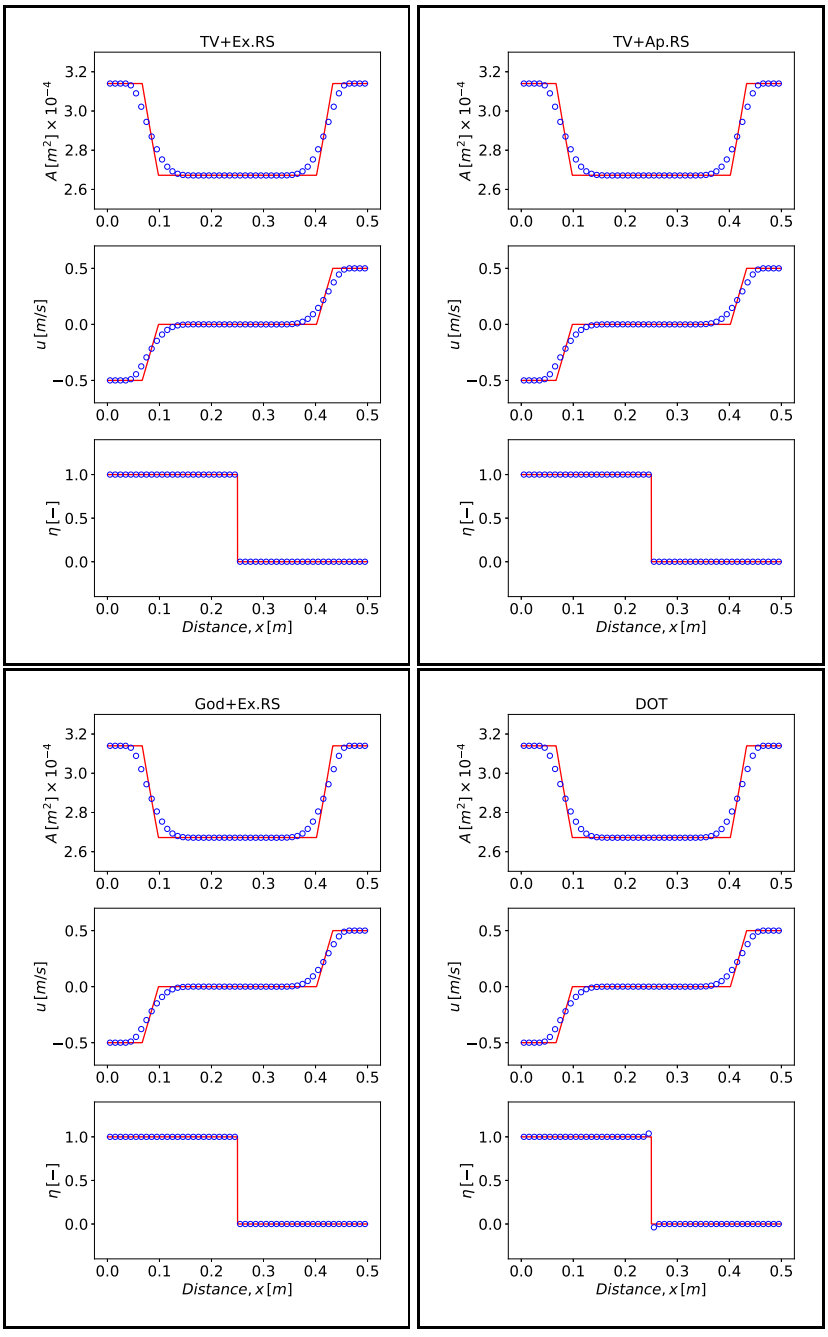

Figure 6: Test 3. Conservative case. Numerical solution from four conservative methods (symbol) compared to the exact solution (line). Top frames show results from the TV-type splitting scheme of this paper in conjunction with the exact Riemann solver (TV+Ex.RS) and an approximate Riemann solver (TV+Ap.RS). The two bottom frames show results from the Godunov method used in conjunction with the exact Riemann solver and from the DOT scheme. $M = 50$ cells, $C_{cfl} = 0.9$. Initial data is given in Table 1 and parameters are given in Table 2.

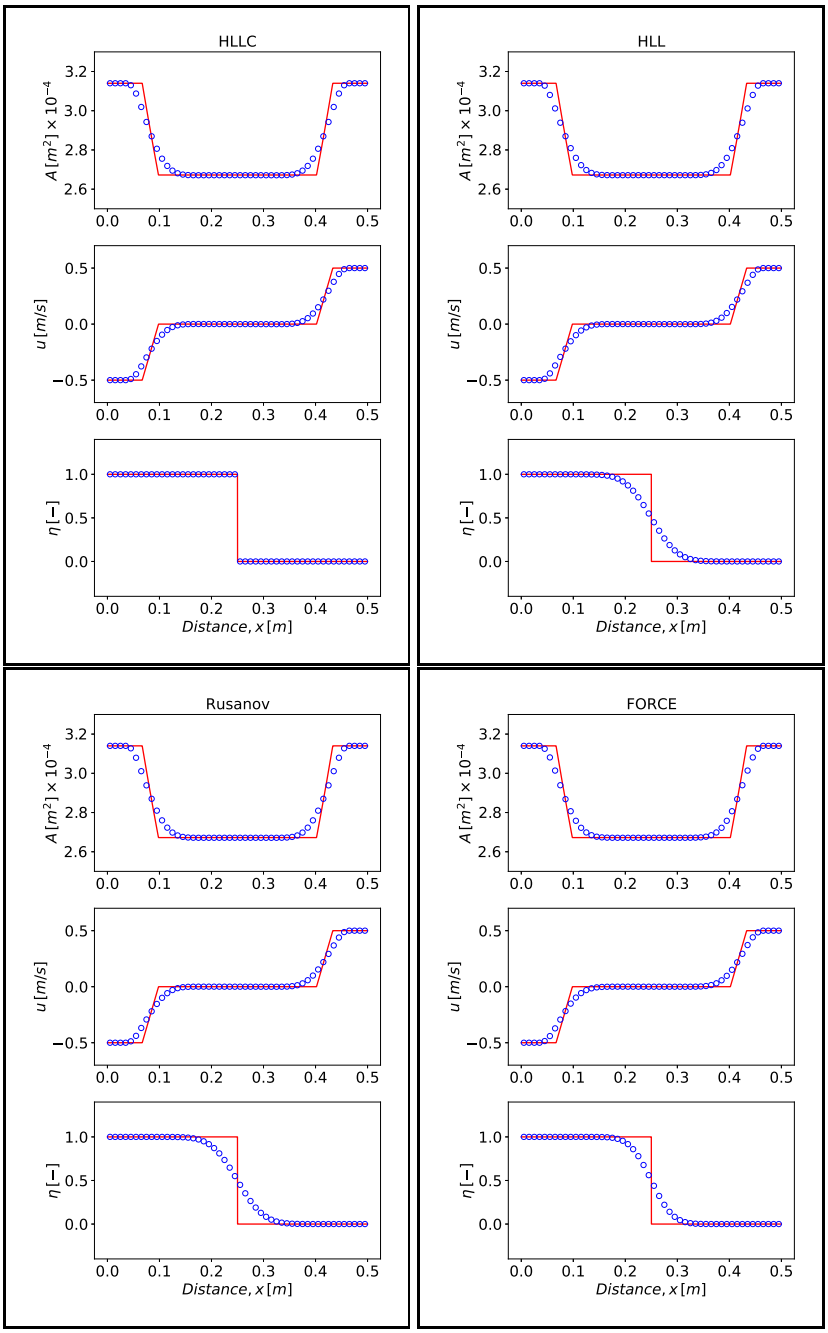

Figure 7: Test 3. Conservative case. Numerical solution from four conservative methods (symbol) compared to the exact solution (line). Top frames show results from the HLLC and HLL schemes. The two bottom frames show results from the Rusanov and the FORCE scheme. $M = 50$ cells, $C_{cfl} = 0.9$. Initial data is given in Table 1 and parameters are given in Table 2.

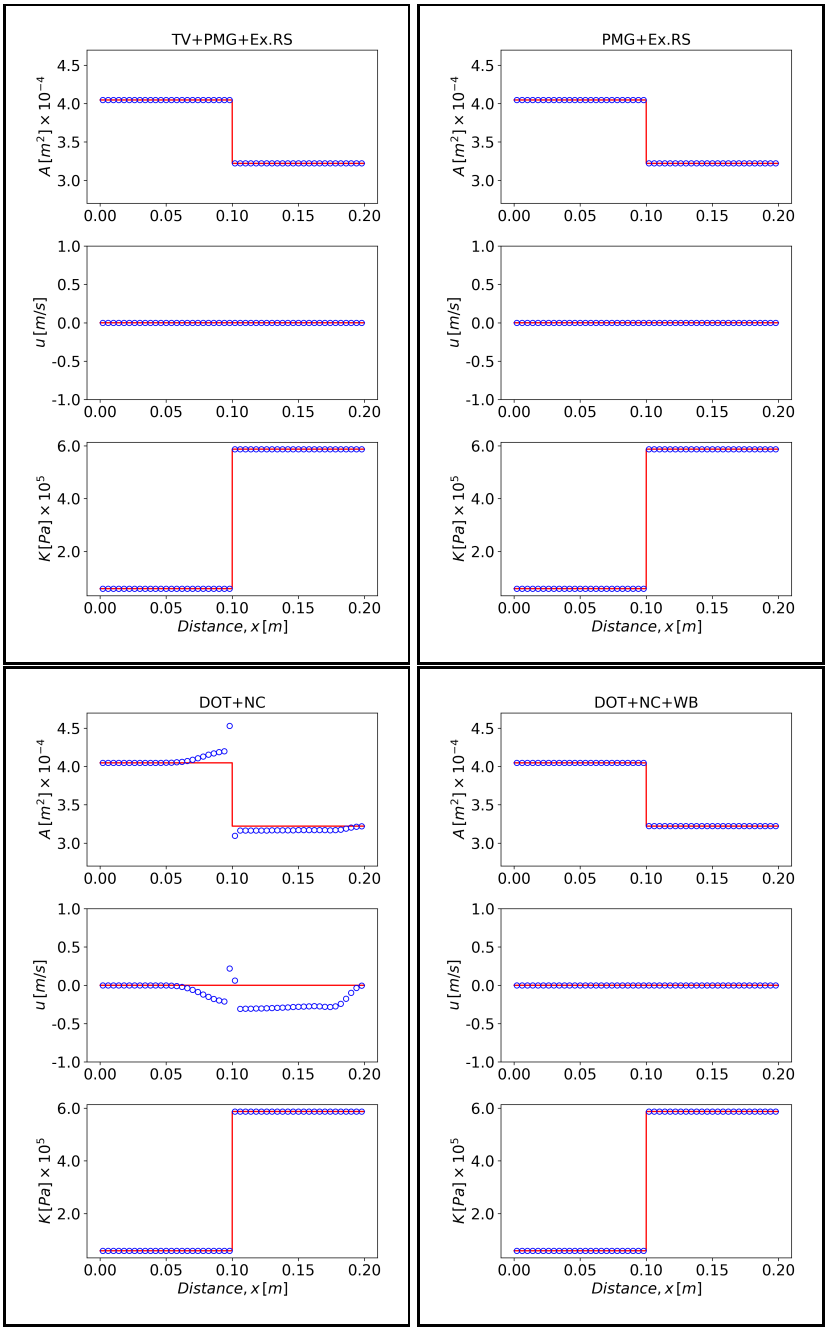

Figure 8: Test 1. Non-conservative case. Numerical solution from four path-conservative methods (symbol) compared to the exact solution (line). The top two frames show results from the TV-type splitting of this paper with the PMG approach in conjunction with the exact Riemann solver (TV+PMG+Ex.RS) and PMG for the full system in conjunction with the exact Riemann solver (PMG+Ex.RS). The two bottom frames show results from the non-conservative versions of the DOT scheme in non-well balanced form (DOT+NC) and in well-balanced form (DT+NC+WB). $M = 50$ cells, $C_{cfl} = 0.9$. Initial data is given in Table 5 and parameters are given in Table 6.

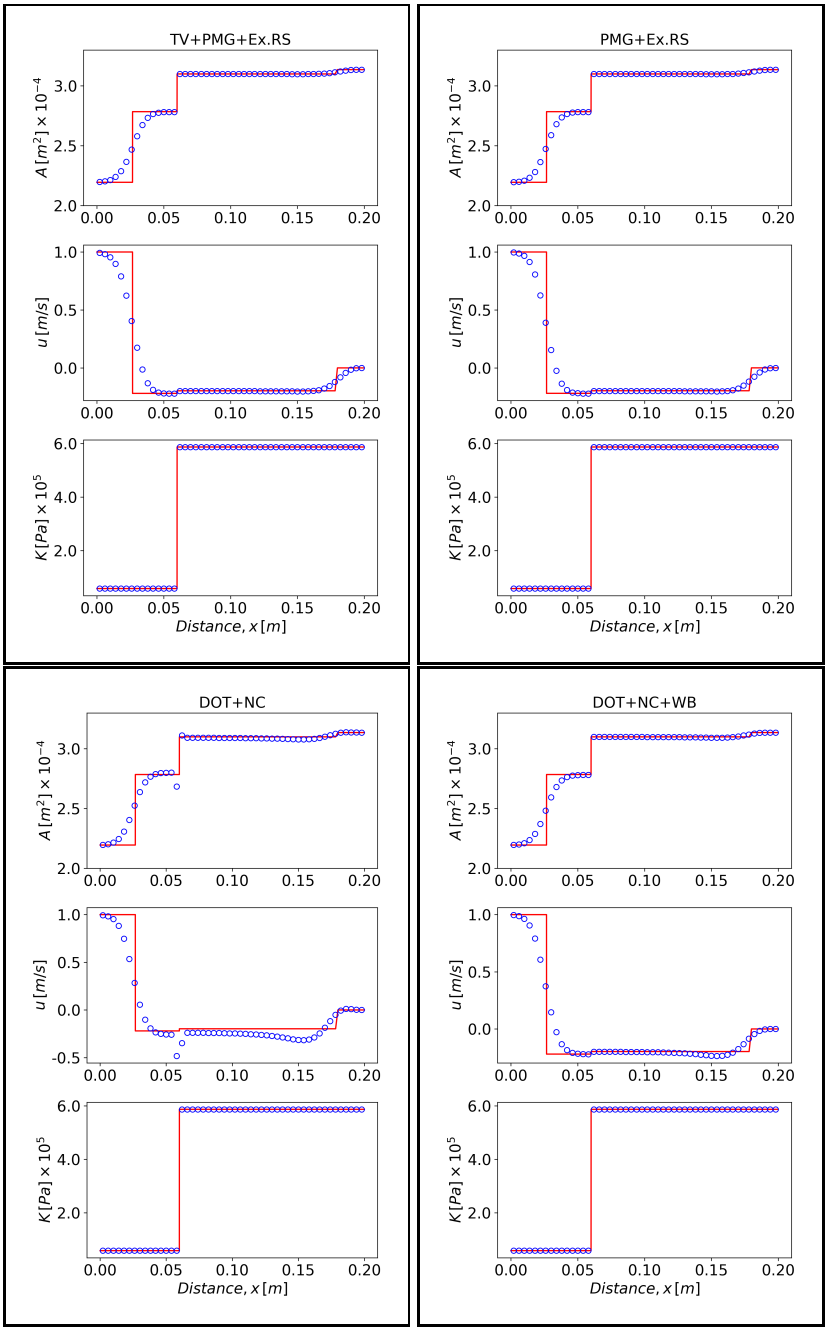

Figure 9: Test 2. Non-conservative case. Numerical solution from four path-conservative methods (symbol) compared to the exact solution (line). The top two frames show results from the TV-type splitting of this paper with the PMG approach in conjunction with the exact Riemann solver (TV+PMG+Ex.RS) and PMG for the full system in conjunction with the exact Riemann solver (PMG+Ex.RS). The two bottom frames show results from the non-conservative versions of the DOT scheme in non-well balanced form (DOT+NC) and in well-balanced (DT+NC+WB). $M = 50$ cells, $C_{cfl} = 0.9$. Initial data is given in Table 5 and parameters are given in Table 6.

ting of this paper with the PMG approach in conjunction with the exact Riemann solver for the pressure system (TV+PMG+Ex.RS). The right frame shows results from PMG for the full system (no splitting) in conjunction with the exact Riemann solver for the full system (PMG+Ex.RS). The two bottom frames show results from the non-conservative version of the DOT scheme in non-well balanced form (DOT+NC) and from the non-conservative well-balanced version (DT+NC+WB). The performance of the new methods shown on the top frames are indeed very satisfactory. They compare very well with those of the sophisticated DOT path-conservative scheme in well-balanced mode (DT+NC+WB). Note however that even the DOT path-conservative scheme fails for this test, unless the well-balanced property is incorporated into the scheme. Of course the outer (left and right) discontinuities are smeared very visibly, which is consistent with first-order mode of all the schemes presented. Note that, apart from DOT+NC, all schemes capture the contact discontinuity with infinite resolution and without spurious oscillations.

6. Concluding Remarks

We have presented a class of very simple advection-pressure splitting numerical methods for solving the equations for blood flow in compliant arterial vessels. The schemes are inspired by the TV flux vector splitting approach for conservative systems proposed by Toro and Vázquez [30] for the compressible Euler equation, but differ from the original scheme in various ways. First, in the present version the continuity equation is fully assigned to the pressure system. This feature is consistent with zero-dimensional models that are based on neglecting the inertial term in the momentum equation, followed by spatial integration. Moreover, the reformulated TV schemes have a wider range of applicability, including systems of equations in non-conservative form, for which there may not be a full flux vector but advection terms with non-conservative products. The TV-type scheme of this paper splits advection terms, which may be in conservative form, from pressure terms in conservative or non-conservative form. The advection-pressure splitting schemes are then implemented in the framework of the Godunov-type path-conservative approach of Parés and Muñoz [14] and are systematically assessed on a suite of carefully designed test problems with exact solution. Moreover, in order to gain a fuller understanding of the potential of the new methods of this paper, they have also been compared against several existing, competitive main-stream methods available in the literature. Overall, we conclude that the proposed numerical methods suggest themselves as attractive computational tools for modelling physiological flows under realistic conditions. Future developments may include extension of the schemes to high-order of accuracy, application to blood flow in compliant venous vessels and to networks composed of both arterial and venous blood vessels to simulate the full human circulatory system.

Acknowledgments

Lucas O. Müller and Alessandra Spilimbergo are members of the Gruppo Nazionale per il Calcolo Scientifico (GNCS) dell' Istituto Nazionale di Alta Matematica (INdAM).

Alessandra Spilimbergo acknowledges the University of Trento for financing her Ph.D. studentship.

References

[1] M.J. Castro, A. Pardo, C. Parés and E.F. Toro, *On some fast well-balanced first order solvers for nonconservative systems*, Math. Comput. **79**(271), 1427–1472 (2010).
[2] M. Dumbser and E.F. Toro, *On universal Osher-type schemes for general nonlinear hyperbolic conservation laws*, Commun. Comput. Phys. **10**(3), 635–671 (2011).
[3] M. Dumbser and E.F. Toro, *A simple extension of the Osher Riemann solver to non-conservative hyperbolic systems*, J. Sci. Comput. **48**, 70–88 (2011).
[4] L. Formaggia and A. Quarteroni, *Cardiovascular Mathematics. Modeling and Simulation of the Circulatory System*, Springer (2009).
[5] O. Frank, *The basic shape of the arterial pulse. First treatise: Mathematical analysis*, J. Mol. Cell. Cardiol. **22**(3), 255–277 (1990).
[6] B. Ghitti, E.F. Toro and L.O. Müller, *Nonlinear lumped-parameter models for blood flow simulations in networks of vessels*, ESAIM Math. Model. Numer. Anal. **56**(5), 1579–1627 (2022).
[7] E. Godlewski and P.A. Raviart, *Numerical Approximation of Hyperbolic Systems of Conservation Laws*, Springer–Verlag (1996).
[8] S.K. Godunov, *A finite difference method for the computation of discontinuous solutions of the equations of fluid dynamics*, Mat. Sb. **47**, 357–393 (1959).
[9] A. Harten, P.D. Lax and B. van Leer, *On upstream differencing and Godunov-type schemes for hyperbolic conservation laws*, SIAM Rev. **25**(1), 35–61 (1983).
[10] R.J. LeVeque, *Finite Volume Methods for Hyperbolic Problems*, Cambridge University Press (2002).
[11] M.S. Liou and C.J. Steffen, *A new flux splitting scheme*, J. Comput. Phys. **107**, 23–39 (1993).
[12] L.O. Müller and E.F. Toro, *Well-balanced high-order solver for blood flow in networks of vessels with variable properties*, Int. J. Numer. Methods Biomed. Eng. **29**, 1388–1411 (2013).
[13] C. Parés, *Numerical methods for nonconservative hyperbolic systems: A theoretical framework*, SIAM J. Numer. Anal. **44**, 300–321 (2006).
[14] C. Parés and M.L. Muñoz Ruíz, *On some difficulties of the numerical approximation of nonconservative hyperbolic systems*, SeMA J. **47**, 19–48 (2009).
[15] A. Quarteroni, M. Tuveri and A. Veneziani, *Computational vascular fluid dynamics: Problems, models and methods*, Comput. Visual. Sci. **2**(4), 163–197 (2000).
[16] V.V. Rusanov, *Calculation of interaction of non-steady shock waves with obstacles*, J. Comput. Math. Phys. USSR **1**, 267–279 (1961).
[17] S. Safaei, P.J. Blanco, L.O. Müller, L.H. Hellevik and P.J. Hunter, *Bond graph model of cerebral circulation: Toward clinically feasible systemic blood flow simulations*, Front. Physiol. **9**, (2018).
[18] A. Siviglia, D. Vanzo and E.F. Toro, *A splitting scheme for the coupled Saint-Venant-Exner model*, Adv. Water Resour. **159**, (2022).
[19] J.L. Steger and R.F. Warming, *Flux vector splitting of the inviscid gasdynamic equations with applications to finite difference methods*, J. Comput. Phys. **40**, 263–293 (1981).
[20] G. Strang, *On the construction and comparison of difference schemes*, SIAM J. Numer. Anal. **5**(3), 506–517 (1968).
[21] E.F. Toro, *Riemann problem based techniques for computing reactive two-phase flows*, in: *Proceedings of the Third International Conference on Numerical Combustion*, A. Dervieux and B. Larrouturrou (Eds), pp. 472–481, Springer-Verlag (1989).
[22] E.F. Toro, *Shock-Capturing Methods for Free-Surface Shallow Flows*, Wiley and Sons (2001).

[23] E.F. Toro, *Riemann Solvers and Numerical Methods for Fluid Dynamics. A Practical Introduction*, Springer–Verlag (2009).
[24] E.F. Toro, *Brain venous haemodynamics, neurological diseases and mathematical modelling. A review*, Appl. Math. Comput. **272**, 542–579 (2016).
[25] E.F. Toro, *The HLLC Riemann solver*, Shock Waves **29**, 1065–1082 (2019).
[26] E.F. Toro and S.J. Billett, *Centred TVD schemes for hyperbolic conservation laws*, IMA J. Numer. Anal. **20**, 47–79 (2000).
[27] E.F. Toro, C.E. Castro, D. Vanzo and A. Siviglia, *A flux-vector splitting scheme for the shallow water equations extended to high-order on unstructured meshes*, Internat. J. Numer. Methods Fluids **94**(10), 1679–1705 (2022).
[28] E.F. Toro and A. Siviglia, *Flow in collapsible tubes with discontinuous mechanical properties: Mathematical model and exact solutions*, Commun. Comput. Phys. **13**(2), 361–385 (2013).
[29] E.F. Toro, M. Spruce and W. Speares, *Restoration of the contact surface in the HLL Riemann solver*, Shock Waves **4**, 25–34 (1994).
[30] E.F. Toro and M.E. Vázquez-Cendón, *Flux splitting schemes for the Euler equations*, Comput. Fluids **70**, 1–12 (2012).
[31] I. Toumi, *A weak formulation of Roe's approximate Riemann solver*, J. Comput. Phys. **102**(2), 360–373 (1992).
[32] B. van Leer, *Flux Vector Splitting for the Euler Equations*, Technical report No 82-30, ICASE (1982).
[33] G.C. Zha and E. Bilgen, *Numerical solution of Euler equations by a new flux vector splitting scheme*, Int. J. Numer. Meth. Fluids **17**, 115–144 (1993).